Fall 2016

An Experimental And Computational Investigation Of The Mechanical, Structural, And Hydrothermal Properties Of Mesoporous Materials

Dayton Gage Kizzire

AN EXPERIMENTAL AND COMPUTATIONAL INVESTIGATION OF THE MECHANICAL, STRUCTURAL, AND HYDROTHERMAL PROPERTIES OF MESOPOROUS MATERIALS

A Masters Thesis

Presented to

The Graduate College of

Missouri State University

In Partial Fulfillment

Of the Requirements for the Degree

Master of Science, Materials Science

By

Dayton G. Kizzire

December 2016

Dayton G. Kizzire

Physics, Astronomy and Materials Science

Missouri State University, December 2016

ABSTRACT

Periodic mesoporous materials have tunable pore sizes and high surface to volume ratios. Some of the most anticipated applications are those that call for energy harvesting in extreme environments, and these materials have a great structural stability to withstand the harsh conditions. In this work, the structural properties of mesoporous materials SBA-15 silica and Al-SBA-15 aluminosilica have been investigated by pressure dependent *in situ* small angle x-ray scattering (SAXS) using a diamond anvil cell (DAC) up to ~12 GPa in pressure. Hydrothermal measurements were also made in this manner to near supercritical water/steam conditions (to 255 °C and ~ 114 MPa) using the DAC. Analysis of the pressure dependent SAXS data yielded bulk modulus values of 12.0 ± 3.0 GPa and 34.7 ± 6.5 GPa for the SBA-15 silica and Al-SBA-15 aluminosilica respectively. The hydrothermal DAC experiment produced results detailing a small net swelling of 1-2% of the pore walls from the dissolution of water into the network structure. The Al-SBA-15 shows significantly greater hydrothermal stability than the SBA-15 silica. In addition, classical molecular dynamics simulations were performed on a series of silica and charge uncompensated aluminosilica amorphous glasses with varying percentage porosity, chemical composition, and onset of pressure at varying temperatures. The simulations were conducted from two types: 1) onset of pressure at the computer-glass transition temperature, and, 2) onset of pressure at room temperature. Within each type, simulations were varied by percentage porosity (0% to 60%) and by aluminum cation percentage (0% to 33%.) These simulations show a decrease in bulk modulus with respect to increasing percentage porosity that follows an exponential decay curve. This is consistent with experimental data from randomly porous materials. The bond angle analysis shows a unique bimodal distribution of Al-O-Al bond angles from the charge uncompensated aluminosilica. This is caused by edge sharing of adjacent tetrahedra due to local charge imbalance created by the substitution of the Al^{3+} ions.

KEYWORDS: aluminosilica, mesoporous, nanomaterial, molecular dynamics, simulations

This abstract is approved as to form and content

_____

Robert A Mayanovic, Ph.D.
Chairperson, Advisory Committee
Missouri State University

AN EXPERIMENTAL AND COMPUTATIONAL INVESTIGATION OF THE MECHANICAL, STRUCTURAL, AND HYDROTHERMAL PROPERTIES OF MESOPOROUS MATERIALS

By

Dayton G. Kizzire

A Masters Thesis
Submitted to the Graduate College
Of Missouri State University
In Partial Fulfillment of the Requirements
For the Degree of Master of Science, Materials Science

December 2016

Approved:

_____
Robert A Mayanovic, Ph.D.

_____
Ridwan Sakidja, Ph.D.

_____
Fei Wang, Ph.D.

_____
Julie Masterson, PhD: Dean, Graduate College

ACKNOWLEDGEMENTS

Firstly, I would like to express my sincere gratitude to my advisor Dr. Robert Mayanovic for the continuous support of my studies and research, for his patience, motivation, and immense knowledge. His guidance has helped me throughout my bachelors and masters research and through the writing of this thesis. I could not have imagined having a better advisor and mentor for my time here at Missouri State University.

I would like to thank Dr. David Cornelison, not only for many years of teaching, but also for mentoring and supporting me the past five years. Dr. Ridwan Sakidja for enlightening me to the world of computational materials science and for spending so much of his time trudging through the basics with me.

I thank my best friends and classmates, Dan Soden and Zach Luety, for all of the stimulating discussions, the enormous amount of French press coffee, and the fun that we have shared in the past five years.

Finally yet importantly, I would love to thank my wife, Farren Kizzire, for the constant love, care, encouragement, and support she has shown me throughout all of my studies and my life in general. In addition to my wife, I would like to thank my parents, Lori and Billy Trimble, for unwavering encouragement, emotional support, and continual love throughout my career and my entire life.

TABLE OF CONTENTS

LIST OF TABLES

LIST OF FIGURES

OVERVIEW

Mesoporous materials are of current interest because of the numerous applications for energy harvesting under extreme environments.[1–4] Some of the most common amongst these materials are silica type (SBA-15, SBA-16, FDU-12, etc.) having amorphous pore walls. Unfortunately, experimental work thus far indicates that mesoporous silica materials of this nature are not ideal for extreme environment energy harvesting applications. The reasons for this are: 1) a lack of stability under extreme pressure and temperature environments, especially under hydrothermal conditions, and, 2) a lack of sufficient catalytic capacity. It has been shown that bulk aluminosilica has much better catalytic properties because of the Lewis acid sites associated with the Al^{3+} catalytic sites, as well as a much higher stability under extreme pressures and high temperature hydrothermal conditions.[5] It is for these reasons that I hypothesized that the mesoporous aluminum type SBA-15, also known as Al-SBA-15, would have a higher stability under extreme pressures and high temperature hydrothermal environments than its silica SBA-15 counterpart. This increased stability would be sufficient to make the material a functional catalyst that would be ideal for extreme environment energy harvesting applications. For commercial energy and industrial applications, it is imperative that the mechanical, thermal, and hydrothermal stability properties of periodic mesoporous silica and aluminosilica under extreme conditions are well understood. Before now, these properties were not well understood and research on these materials had only been conducted in boiling water or steam environments, but not in the

supercritical solutions that are necessary for energy harvesting under extreme environments.

Although the objective of this work is on the characterization and computational modeling of select mesoporous materials (the synthesis of the SBA-15 silica and the Al-SBA-15 aluminosilica was carried out in Prof. Kai Landskron's laboratory at Lehigh University), it is instructive to provide a short background on the synthesis of this class of self-assembled materials. Synthesis of mesoporous materials has undergone explosive growth since the inception of the first MCM materials in 1992.[6] Surfactant-templated self-assembly has proven to be a versatile synthetic tool for the synthesis of numerous metal oxides from metal alkoxide precursors and surfactants in aqueous solutions and even some non-oxidic mesoporous materials like mesoporous carbons have been made this way.[7] The wide range of ionic and non-ionic surfactants that can be used as templates have led to mesoporous materials with many different pore systems and tunable pore sizes. The surfactant-templated self-assembly has been complemented by the nanocasting strategy (see Fig. 1).[8] In this approach, a mesoporous material is infiltrated by a precursor of the target material and then the precursor is converted inside the pores to form the

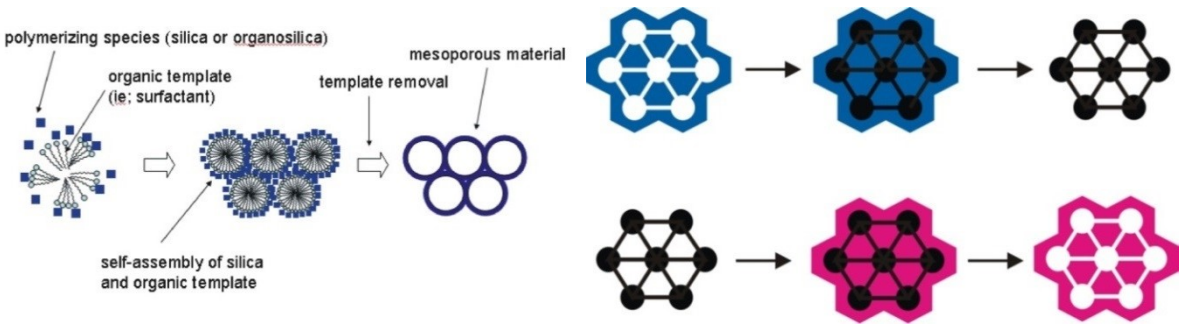

Fig. 1 (left): *The soft-templating method. A hydrolyzed oxidic precursor (squares) co-assembles with an amphiphilic surfactant template to form a mesostructured composite. The nanocomposite can be transformed into a periodic mesoporous oxide material by template removal.* ***Fig. 1 (right):*** *The nanocasting process. A periodic mesoporous material (e.g. mesoporous silica SBA-15; blue) is inverted into a negative replica (black) by nanocasting. Infiltration of sucrose into the pores of SBA-15 and carbonization of the sugar produces a carbon/silica composite (blue-black.) Selective etching of the carbon/silica nanocomposite with HF gives the mesoporous carbon (black). The so-prepared negative carbon replica can be used as hard template for the preparation of other periodic mesoporous materials (red)*

target material. In the last step, the hard template is removed by a suitable method. The nanocasting strategy offers more control over the pore system because the product mesopore structure is the inverse of the template structure and is not bound to aqueous solutions. based nanocomposites and many others. It has recently been shown that mesoporous nitridic materials can be synthesized by melt-infiltration of hexachlorocyclotriphosphazene into mesoporous silicas.[9] Fig. 1 illustrates the soft-templating method used to synthesize the SBA-15 silica and the Al-SBA-15 aluminosilica used in this study.

My objective in this work is to combine experimental characterization and computational modeling in order to provide a better understanding of the correlations between type (i.e, silica vs aluminosilica) and network structure of the atomic constituents in governing the stability of periodic mesoporous materials under extreme pressures and under high pressure-temperature conditions in a hydrothermal environment. The computational modeling will provide insight into the atomistic and structural properties, such as bond angles, bond angle deformations, and coordination numbers, that are not accessible from experimental characterization. The computational modeling for this work is best done with classical molecular dynamics simulations using readily available interatomic potentials. Due to the large size of the computational cell required for this work, it is necessary to use large parallel architecture computing facilities, such as those available through the Extreme Science and Engineering Discovery Environment (XSEDE) and through the Texas Advanced Computing Center (TACC). The complementary experimental characterization involves making *in situ* small angle x-ray scattering (SAXS) measurements at synchrotron facilities. Additional *ex situ*

characterization involves transmission electron spectroscopy (TEM), scanning electron microscopy (SEM), and x-ray photoelectron microscopy (XPS).

In this thesis I will present experimental data on the structural stability of the mesoporous materials Al-SBA-15 and SBA-15 under extreme pressures in the form of a normalized bulk modulus and hydrothermal stability measurements detailing the dissolution of the mesoporous framework in supercritical water. In addition, I will present computational results that show the change of structural stability of silica and aluminosilica due to varying initial conditions of percentage porosity and percentage of aluminum cations.

INVESTIGATIONS OF THE MECHANICAL AND HYDROTHERMAL STABILITIES OF SBA-15 AND AL-SBA-15 MESOPOROUS MATERIALS

Abstract

Periodic mesoporous materials possess high surface to volume ratio and nano-scale sized pores, making them potential candidates for heterogeneous catalysis, ion exchange, gas sensing and other applications. In this study, I use *in situ* small angle x-ray scattering (SAXS) and molecular dynamics (MD) simulations to investigate the mechanical and hydrothermal stability properties of periodic mesoporous SBA-15 silica and SBA-15 type aluminosilica (Al-SBA-15) to extreme conditions. The mesoporous SBA-15 silica and Al-SBA-15 aluminosilica possess amorphous frameworks and have similar pore size distribution (pore size ~9-10 nm). The *in situ* SAXS measurements were made at the B1 beamline, at the Cornell High Energy Synchrotron Source (CHESS). The mesoporous SBA-15 silica and Al-SBA-15 aluminosilica specimens were loaded in a diamond anvil cell (DAC) for pressure measurements, and, separately, with water in the DAC for hydrothermal measurements to high P-T conditions (to 255 °C and ~ 114 MPa). Analyses of the pressure-dependent SAXS data show that the mesoporous Al-SBA-15 aluminosilica is substantially more mechanically stable than the SBA-15 silica. Hydrothermal measurements show a small net swelling of the framework at elevated P-T conditions, due to dissolution of water into the pore walls. Under elevated P-T conditions, the Al-SBA-15 aluminosilica shows significantly greater hydrothermal stability than the SBA-15 silica. My MD simulations show that the bulk modulus value of periodic mesoporous SBA-15 silica varies exponentially with percentage porosity. Molecular

dynamics simulations are being made in order to better understand how the pore architecture and the chemical composition of the host structure govern the stability properties of the mesoporous materials.

Introduction

Periodic mesoporous SBA-15 silica and Al-SBA-15 aluminosilica hold great interest because of their unique characteristics of tunable pore sizes and high surface area give them potential for applications in heterogeneous catalysis, ion exchange, gas sensing, fuel cells, batteries, and biomass gasification [1-3]. Many of these applications are envisioned for extreme or high temperature conditions. In order to perform well in extreme environments, the mesoporous silica and aluminosilica materials need to have considerably higher mechanical, thermal, and hydrothermal stability characteristics. Ordered mesoporous materials having aluminosilicate frameworks are of special interest because the presence of Al^{3+} creates active sites for catalysis (e.g., Lewis acid sites) and ion exchange. Furthermore, aluminosilica mesoporous materials hold promise for exhibiting better stability under extreme hydrothermal conditions than mesoporous silica [4]. The objective of this work is to provide a better understanding of the correlations between type (i.e, silica vs aluminosilica) and network structure of the atomic constituents in governing the stability of periodic mesoporous materials under extreme pressures and under high pressure-temperature conditions in a hydrothermal environment. In this paper, I discuss my experiments on the mechanical and extreme hydrothermal stability of the SBA-15 silica and the Al-SBA-15 aluminosilica materials. In addition, I discuss my initial molecular dynamic simulations of the mechanical response of SBA-15-

type silica to hydrostatic pressure through the calculations of the bulk modulus values against the percentage porosity of the mesoporous material.

Experimental

The SBA-15 silica and SBA-15-type aluminosilica (Al-SBA-15) were synthesized at Lehigh University using a soft templating method according to literature procedures [5]. The *in situ* small angle x-ray scattering (SAXS) measurements were made at the B1 beam line, at the Cornell High Energy Synchrotron Source (CHESS). The 25.51 keV x-rays were collimated to a beam size of ~ 100 μm in diameter. A 125 μm thick Re gasket (~ 250 μm i.d.) was used to load the sample in the diamond anvil cell (DAC): The samples were loaded in an argon environment along with a small ruby crystal pressure calibrant, for pressure-dependent SAXS measurements. The x-rays were incident on the sample parallel to the compression axis of the DAC (see Figure 1.1). The x-rays scattered from the sample were imaged using a MAR345 image plate detector placed at ~1134.6 mm from the sample. The SAXS images (see Figure 1.1) were processed using Fit2d software [6]. For *in situ* SAXS measurements under extreme hydrothermal conditions, the sample was loaded along with deionized water in the sample volume defined by a 250 μm thick Re gasket (~ 500 μm i.d.) and anvils in the DAC. Upon heating of the sample using an internal resistance heater in the DAC, the liquid-vapor homogenization temperature (T_h) was used to determine the fluid density of the aqueous fluid and thereby estimate the pressure of the sample at $T > T_h$ through calculations using the equation of state of water [7].

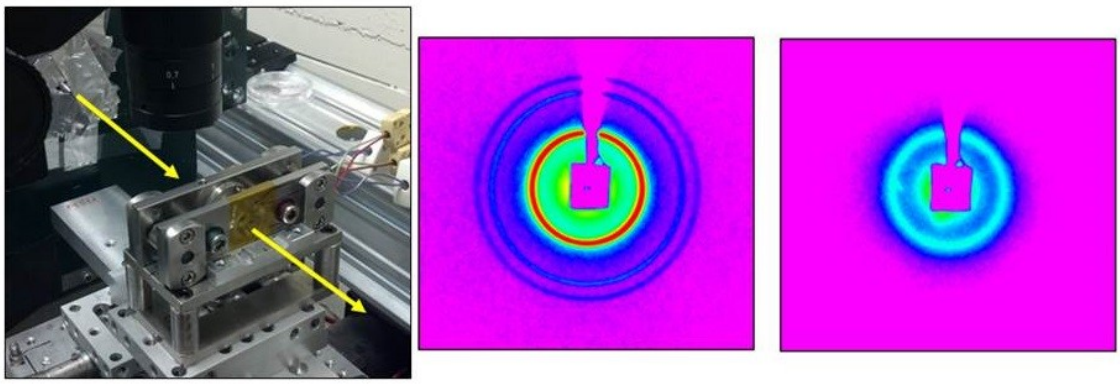

Figure 1.1: (**Left**) Diamond Anvil Cell experimental setup with the arrows indicating the path of the x-ray beam through the DAC. (**Right**) Resulting SAXS diffraction images measured from the Al-SBA-15 mesoporous aluminosilica at 0.1 GPa (middle) and 2.1 GPa (extreme right).

Results and Discussion

Figure 1.1 shows the SAXS diffraction images measured from the Al-SBA-15 mesoporous aluminosilica under high pressure conditions. In Figure 2 are shown the *in situ* angle-dependent SAXS data measured from the Al-SBA-15 mesoporous aluminosilica as function of pressure at 25 °C. From these results I see that the extended range of pore structure ordering persists to approximately 1.4 GPa and that there is significant pore collapse between 3.5 to 11.2 GPa. The *in situ* SAXS data measured from the SBA-15 mesoporous silica as function of pressure at 25 °C are similar in appearance but the SAXS signal degrades more appreciably under high pressure conditions. For SBA-15 silica, the extended range of pore structure persists to approximately 1 GPa whereas pore collapse is evident at close to 4 GPa. Both the SBA-15 silica and Al-SBA-15 aluminosilica have a 2D hexagonal pore (p6mm space group) structure symmetry as determined by the first:second and second:third ratios of the 2θ positions of the SAXS data (see Figures 2 and 3). The pressure-dependent volume of the pore structure unit cell

(V_P) was determined by fitting a Gaussian peak-shape to the background subtracted (100) x-ray scattering peak occurring near $2\theta \sim 0.28°$: The unit cell only has an area dimension but because the samples were exposed to hydrostatic-like pressure conditions, I have adopted a volume-like description having an aribtrary dimension perpendicular to the plane containing the 2D hexagonal pore structure. The fractional change in the pore-structure unit cell volume (V_P/V_0) is calculated by taking the ratio of V_P, which is the volume at pressure P, to $V_{0,}$ which is the volume at 0.1 MPa. The V_P/V_0 vs pressure data for the Al-SBA-15 mesoporous aluminosilica sample are shown in Figure 1.2. The bulk modulus was calculated from the slope of the linear fits made in the elastic region of the plot of the fractional change in the pore-structure unit cell volume (V_P/V_0) vs pressure (see Figure 2).

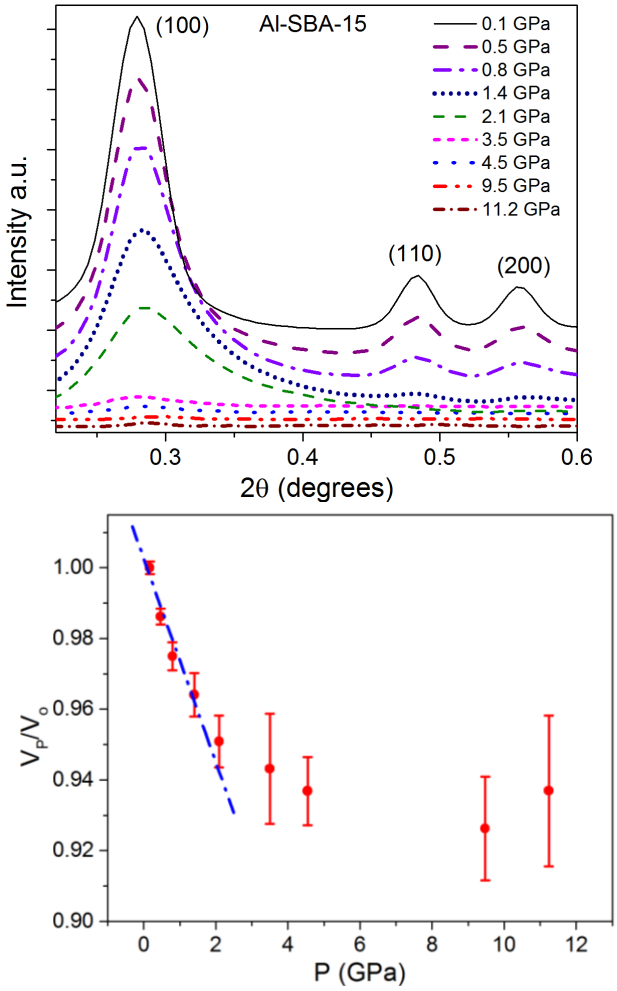

Figure 1.2: (**Top**) I vs. 2θ of pressure measurements conducted on Al-SBA-15. (**Bottom**) Fractional change in pore-structure unit cell volume (V_P/V_0) of the mesoporous Al-SBA-15 aluminosilica as a function of pressure (P).

The estimated bulk modulus of the materials was found to be significantly different for the two materials. The Al-SBA-15 type aluminosilica periodic mesoporous material has a bulk modulus 34.7 ± 6.5 GPa whereas the SBA-15 type silica mesoporous material has a considerably smaller bulk modulus 12.0 ± 3.0 GPa. In Al-SBA-15, a significant portion of the Si^{4+} ions are replaced by Al^{3+} within the framework of the mesoporous architecture creating a local charge-imbalance and thereby affecting the strength of the local Al–O bonds. The primary mechanical response within the elastic region of Al-SBA-15 mesoporous aluminosilica is expected to result from T–O–T (T =

Si, Al) bond bending occurring at the bridging oxygen site. The Si–O–Al bond angles have been known to be softer (against bending) than the Si–O–Si bond angles in minerals, and furthermore appear to depend upon the number of atoms the bridging O is linked to (i.e., stiffness increases with number of linked atoms) [8]. Clearly, there are potentially a number of contributions to the mechanical response, including the role of the pore wall surfaces and pore architecture that yield a relatively high bulk modulus for Al-SBA-15 type aluminosilica. More experimental and computational modeling work is required to better understand the mechanical stability of aluminosilica-base mesoporous materials.

In Figure 1.3 I show the *in situ* SAXS data measured from the Al-SBA-15 mesoporous aluminosilica under extreme hydrothermal conditions to 255 °C and 114 MPa. Similar *in situ* SAXS measurements from mesoporous SBA-15 silica made under extreme hydrothermal conditions (to 200 °C and 2 MPa) reveal that this material exhibits similar characteristics but with a greater degradation of pore structure at 200 °C, thus exhibiting less hydrothermal stability. Analysis of the (100) peak in the *in situ* SAXS data, after taking into account thermal expansion and pressure-related volume contraction effects, reveals approximately a 1% and 2% increase of the pore unit cell volume for SBA-15 silica and Al-SBA-15 aluminosilica, respectively, at 200 °C. This is comparable to the expansion of the pore structure unit cell volume (3% at 300 °C and 160 MPa) in our FDU-12 type silica measured under extreme hydrothermal conditions [9]. This indicates incorporation of water into the framework (i.e., pore walls) of the mesoporous silica and aluminosilica under extreme hydrothermal conditions. I have attributed this effect previously, in the case of FDU-12 type mesoporous silica, to the hydrolysis of Si–

O–Si bonds and formation of Si–OH units within the amorphous silica matrix of the pore walls [9]. In the case of Al-SBA-15 type aluminosilica, in addition to Si–O–Si bond breaking and Si–OH bond formation, we must also consider Si–O–Al and Al–O–Al bond breaking and Al–OH bond formation. It is plausible that some water incorporation (in the pore walls) also occurs simply due to filling of the voids. The T–O–T bond breaking results in the deterioration of the pore structure of SBA-15 type silica and Al-SBA-15 type aluminosilica under hydrothermal conditions.

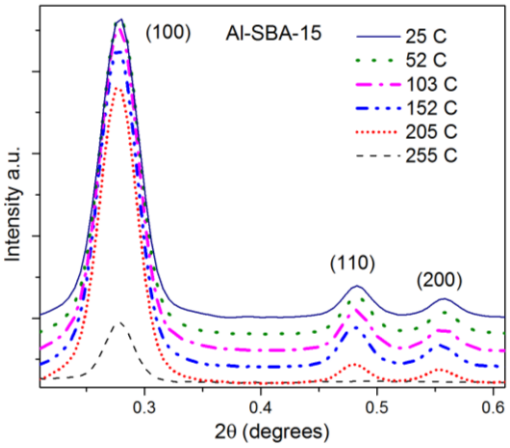

Figure 1.3: Intensity vs. 2θ plot of Al-SBA-15 as a function of temperature in an extreme hydrothermal environment.

I have also carried out molecular dynamic (MD) simulations of the mechanical response of mesoporous silica under hydrostatic pressure conditions. The MD simulations were conducted using LAMMPS software and the parameterized Si–O Tersoff potential [10], in order to run NPT simulations of mesoporous silica under pressure. The resulting data was extensively analyzed to gain a better understanding of the mechanical properties of the mesoporous materials. In order to utilize more computing power, supercomputers through the XSEDE and NERSC were used. The

simulations were performed on four different simulation cells with various porosities: 0% (i.e., bulk silica), 3%, 19%, and 29%. In Figure 4, the illustration on the left shows an image of the simulation cell used for MD simulation of the mesoporous silica having the 2D hexagonal pore structure with 19% porosity.

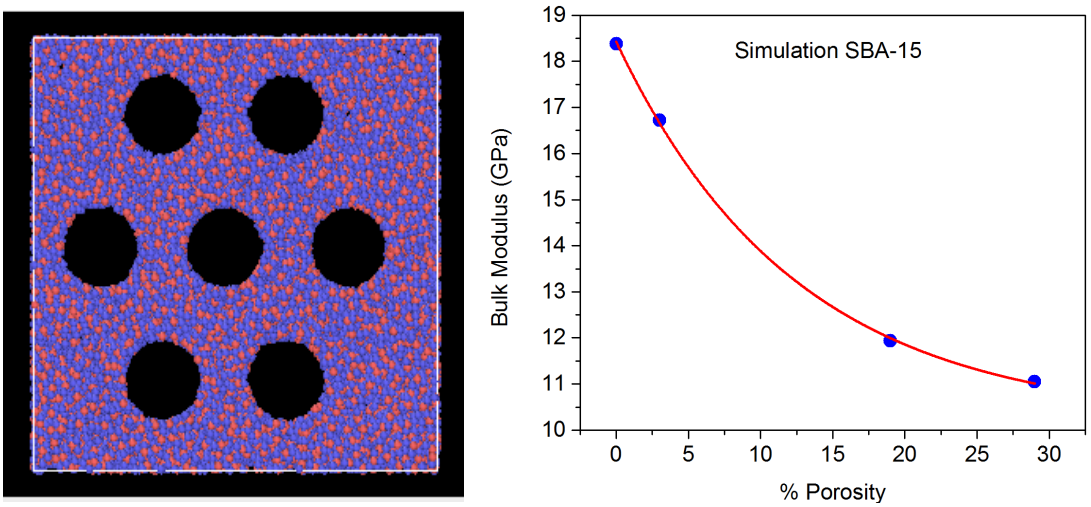

Figure 1.4: (**Left**) MD simulation image of 19% porosity of 2D hexagonal pore-structued SBA-15 silica. (**Right**) A plot of the bulk modulus of mesoporous SBA-15 type silica vs percentage porosity.

The bulk modulus vs % porosity has an exponential decay dependence, which is consistent with the mechanical stability of non-periodic and randomly porous materials. Compared to experiment however, the bulk modulus value for the bulk sample (~18 GPa) is much lower than the accepted experimental values (~33-37 GPa). I believe this is due to the quick cooling rate (~ 10^{11} K/s) that was employed to generate the glass-like structures, which would typically result in a relatively large molar volume of the glass and consequently a lower bulk modulus in the MD simulation results. I also note that the Tersoff potential parameters developed in reference [10] had not been optimized to evaluate the high pressure effects. In addition, the Coulombic interactions were neglected

during the MD simulations. Nevertheless, the observation of a large reduction in the bulk modulus with increasing % porosity for the MD simulated silica glasses are along expected lines and the trend is similar to my experimental findings from *in situ* SAXS data.

Conclusions

In situ SAXS measurements have been made of mesoporous SBA-15 silica and Al-SBA-15 aluminosilica having the 2D hexagonal pore structure (p6mm) at high pressure conditions and under extreme hydrothermal conditions. The estimated bulk modulus of periodic mesoporous Al-SBA-15 aluminosilica is 34.7 ± 6.5 GPa whereas SBA-15 silica has a much lower bulk modulus of 12.0 ± 3.0 GPa. The Al-SBA-15 aluminosilica exhibits greater stability under extreme hydrothermal conditions (to 255 °C, 114 MPa) as compared to SBA-15 silica. My molecular dynamics simulations of mesoporous silica (SBA-15 type) having 2D hexagonal pore structure show that the bulk modulus exhibits an exponential dependence on percent porosity.

Acknowledgements

S.D., R.A.M., K.L., and M.M. acknowledge partial support from EFree, an Energy Frontier Research Center funded by the US Department of Energy, Office of Science, Office of Basic Energy Sciences under Award Number DE-SC0001057. The x-ray scattering was conducted at the Cornell High Energy Synchrotron Source, which is supported by the National Science Foundation and the National Institutes of Health/National Institutes of General Medical Sciences under NSF award DMR-1332208.

References

1. A. Corma, *Chem. Rev.* **97**, 2373-2419 (1997**)**.

2. G.J. de A.A. Soller-Illia, C. Sanchez, B. Lebeau, J. Patarin, *Chem. Rev.* **102**, 4093-4138 (2002**)**.

3. Z.A. ALOthman, Materials **5**, 2874-2902 (2012).

4. R. Mokaya, Adv. Mater. **12**, 1681-1685 (2000).

5. M. Mandal, A.S. Manchanda, C. Liu, Y. Fei, K. Landskron, *RSC Advances* **6**, 7396-7402 (2016).

6. A.P. Hammersley, *Eur. Synchrotron Radiat. Facil. Intern. Rep. ESRF97HA02T*, 1997.

7. W. Wagner, A.J. Pruß, Phys. Chem. Ref. Data 31 (2002) 387-535.

8. R. Downs, H. Yang, R.M. Hazen, L.W. Finger, C.T. Prewitt, Am. Mineral. 84, 333–340 (1999).

9. R.A. Mayanovic, H. Yan, A.D. Brandt, Z. Wang, M. Mandal, K. Landskron, W.A. Bassett, Micorporous Mesoporous Mater. 195 (2014) 161-166.

10. S. Mumetoh, T. Mootoka, K. Moroguchi, A. Shintani, *Comp. Mat. Sci.*, **39,** 334-339 (2007).

STUDIES OF THE MECHANICAL AND EXTREME HYDROTHERMAL PROPERTIES OF PERIODIC MESOPOROUS SILICA AND ALUMINOSILICA MATERIALS

Abstract

Periodic mesoporous SBA-15 silica and Al-SBA-15 aluminosilica have potential for applications in the energy and chemical industries. The pore structure and mechanical properties of periodic mesoporous silica SBA-15 and periodic mesoporous aluminosilica Al-SBA-15 are investigated using *in situ* small angle x-ray scattering (SAXS), transmission electron microscopy (TEM), and x-ray photoelectron spectroscopy (XPS). The SAXS measurements were made at the Cornell High Energy Synchrotron Source (CHESS). The pressure-dependent SAXS measurements were made on mesoporous SBA-15 silica and Al-SBA-15 aluminosilica samples using a diamond anvil cell (DAC) to ~ 12 GPa in pressure. *In situ* SAXS measurements were also made of the mesoporous SBA-15 silica and Al-SBA-15 aluminosilica under extreme hydrothermal conditions (to 255 °C and ~ 114 MPa) using the diamond anvil cell (DAC). TEM image analysis and x-ray diffraction show that the SBA-15 and Al-SBA-15 possess amorphous pore walls and have similar pore size distribution. Analyses of the pressure-dependent SAXS data show that the mesoporous Al-SBA-15 aluminosilica has substantially greater mechanical stability than the mesoporous SBA-15 silica. Analysis of the hydrothermal SAXS data displays a small net expansion of the pore walls in near supercritical aqueous environments that is more significant (~ 2x percentage wise) in Al-SBA-15 aluminosilica than in SBA-15 silica. Amid extreme, near supercritical aqueous environments, the Al-

SBA-15 aluminosilica exhibits superior hydrothermal stability compared to SBA-15 silica.

Introduction

Periodic mesoporous sieves are attractive materials for industrial and commercial applications due to their inherent high surface area and controllable pore size. The high surface-to-volume ratio in these materials and nano-scale (2 nm < diameter < 50 nm) pores make them potential candidates for heterogeneous catalysis, ion exchange, gas sensing and other applications.[1–5] In particular, periodic mesoporous silica, which was the first self-assembled material having ordered pores to be synthesized, are currently still of wide interest due to their tunability and potential for applications. Well-ordered mesoporous materials having aluminosilica pore walls are also currently of interest due to the active Al^{3+} catalytic sites (e.g., Lewis acid sites) contained within the pore surfaces. The development of mesoporous silica- and aluminosilica-based materials for energy conversion and harnessing applications is particularly desired. The common element of many of these targeted energy applications, such as petrochemical refinement, biomass gasification in supercritical water, and high-temperature fuel cells, is the use of extreme conditions as operating variables.

For energy and industrial applications, it is vital that the stability properties (e.g., mechanical, thermal, and hydrothermal) of periodic mesoporous silica and aluminosilica under extreme conditions are well understood. Several different types of ordered mesoporous silica materials have been shown to exhibit a high degree of mechanical stability under quasi-hydrostatic pressure;[6,7] the authors are not aware of such studies made on mesoporous aluminosilica in the past. The majority of previous studies of

hydrothermal stability of silica and aluminosilica mesoporous materials have been limited predominantly to experiments made in boiling water or steam conditions which yield useful data but are not representative of the extreme conditions in supercritical aqueous-based solutions. Using in situ small angle x-ray scattering (SAXS), Mayanovic et al. found that FDU-12 type mesoporous silica becomes irreversibly disordered upon exposure to water at 300 °C and 160 MPa.[6] Conversely, exposure to boiling water experiments have shown that mesoporous aluminosilica materials have somewhat better promise for being stable under extreme hydrothermal conditions.[8,9] Similarly, Wang et al. discovered from boiling water experiments that structural incorporation of Al atoms into the pore wall surfaces of MCM-48 silica improved its hydrothermal stability.[10] Nevertheless, the correlations between the chemical composition, the atomic-scale structure and the pore structure in governing the mechanical, (hydro)thermal, and other physicochemical properties of mesoporous materials are not understood. In the first-of-its kind study presented herein, I examine the mechanical stability under quasi-hydrostatic pressure and the stability under extreme hydrothermal conditions (to 255 °C and 114 MPa) of SBA-15 type mesoporous silica and of SBA-15 type mesoporous aluminosilica (Al-SBA-15). By using in situ SAXS measurements and molecular dynamics (MD) simulations modeling, I aim to understand how the chemical composition, for a given pore structure (2d-dimensional *p6mm* hexagonal) and architecture, and atomic-scale (disordered) structure combine to govern the mechanical and hydrothermal stability properties of SBA-15 silica and Al-SBA-15 aluminosilica.

Experimental

I used commercially available triblock copolymer Pluronic F127 (BASF) and tetraethyl orthosilicate (Sigma-Aldrich) to synthesize the mesoporous SBA-15 silica. Synthesis of periodic mesoporous SBA-15 silica was made using Pluronic F127 ($EO_{106}PO_{70}EO_{106}$) as a structure directing agent and tetraethyl orthosilicate (TEOS) as a silica source according to procedures described in the literature.[11] First, 0.5 g of Pluronic F127 was dissolved in 30 ml of 2.0 M HCl aqueous solution. Next, the solution was magnetically stirred at 15 °C to complete dissolution of the polymer. Subsequently, 0.60 g of mesitylene and 2.5 g of KCl were added and, allowed to rest for two hours, after which 2.08 g of TEOS was added to the mixture and stirred thoroughly for 1 day. The aqueous solution/mixture was hydrothermally treated at 100 °C for 1 day. The resulting SBA-15 material was subsequently collected by centrifuging and then washed with deionized water and dried in air. The as-synthesized dried material was then calcined at 550 °C for 5 h under air (heating rate 2 °C/min).

The mesoporous Al-SBA-15 aluminosilica was synthesized using the pH adjusting method outlined previously.[12,13] A measure of 0.8 g of Pluronic P123 ($EO_{20}PO_{70}EO_{20}$) blockcopolymer was dissolved in 25 ml of 2 M HCl solution and magnetically stirred at 40 °C to complete dissolution. Next, 1.7 g of tetraethoxysilane (Gelest) was added to the solution and stirred for 4 hours, after which 1.36 g of $Al_2(SO_4)_3{\cdot}xH_2O$, x~14-18, (Alfa Aesar) were added and the mixture was stirred for 1 day at 40 °C. Subsequently, the mixture was hydrothermally treated at 100 °C for 2 days. After the hydrothermal treatment, the pH of the mixture was adjusted to about 7.5 using drops of concentrated NH_4OH solution. The mixture was further treated hydrothermally

(at 100 °C) for 2 days. After the second hydrothermal treatment, the material was centrifuged and then washed with deionized water and subsequently allowed to dry. In the final step, removal of the surfactant was accomplished by calcination of the final product in air at 550 °C (at a heating rate of 2 °C per minute) for 5 h.

The SAXS measurements were made at the B1 beam line, at the Cornell High Energy Synchrotron Source (CHESS). The high energy x-rays (25.5 keV) were collimated to a beam size of ~ 100 μm in diameter. For pressure measurements, a Re gasket with diameter ~ 200 μm was placed on top of the culet face of the bottom anvil of the diamond anvil cell (DAC), loaded with a sample and then sealed by pressing the top anvil and secured with tightening screws. The loading of the samples were made in an argon environment and a small piece of ruby crystal was placed with the sample for the high pressure portion of the experiment. The shift in the B2 fluorescence line of ruby was used to gauge the pressure of the sample in the DAC. As shown in Figure 1a), the x-rays were incident on the sample parallel to the compression axis of the DAC. The x-rays scattered from the sample were imaged using a MAR345 image plate detector (Figure 2) placed at ~ 1134.6 mm from the sample. The SAXS images were processed using Fit2d software[14] to produce the intensity (I) of SAXS vs Q data, where $Q = 4\pi\sin\theta/\lambda$, 2θ is scattering angle, and λ (0.48608 Å) is the incident wavelength. For hydrothermal experiments, the sample was loaded along with deionized water in the sample volume defined by the hole in the Re gasket (~ 300 μm) and anvils in the DAC. Each sample was loaded in the sample chamber of the cell so as to contain an appropriately sized small vapor bubble. The liquid-vapor homogenization temperature (T_h), used to determine the fluid density of the aqueous fluid, was recorded for each sample by watching the

disappearance of the vapor bubble in the sample using a microscope. Upon heating above T_h, the pressure follows an isochore that is determined by the fluid density, sample temperature and the T_h value. The estimated pressures were calculated using the equation of state of water[15] and the T_h and temperature values. The SBA-15 silica and Al-SBA-15 aluminosilica samples were held under hydrothermal conditions for ~ 4 hr 30 min and ~ 3 hr 20 min, respectively.

Scanning electron microscopy was made using an FEI Quanta 200 FEG Scanning Electron Microscope (SEM). Energy dispersive x-ray spectroscopy (SEM-EDX) was made using focused electron beam at 20 keV. Samples of the SBA-15 silica and Al-SBA-15 aluminosilica were prepared for transmission electron microscopy (TEM) by dispersal in hexane and subsequent deposition on lacey carbon grid. TEM analysis was made at the University of Arkansas Nano-Bio Materials Characterization Facility using a Titan 80-300 operating at 300 keV. Measurement of pore and pore wall dimensions from the TEM images was made using imageJ[16] software. X-ray photoelectron spectroscopy (XPS) was made on the mesoporous materials for surface compositional analysis. The XPS was performed using a Thermo Electron North America system with an Al K-alpha source of 1486.6 eV characteristic energy. The source and analyzer were calibrated using the Ag $3d_{5/2}$ peaks. I used the CasaXPS 2.3.16 software for peak fit analysis of the XPS spectra. The Shirley type background was used exclusively during the XPS peak fitting analysis. Additional experimental details are provided elsewhere.[17]

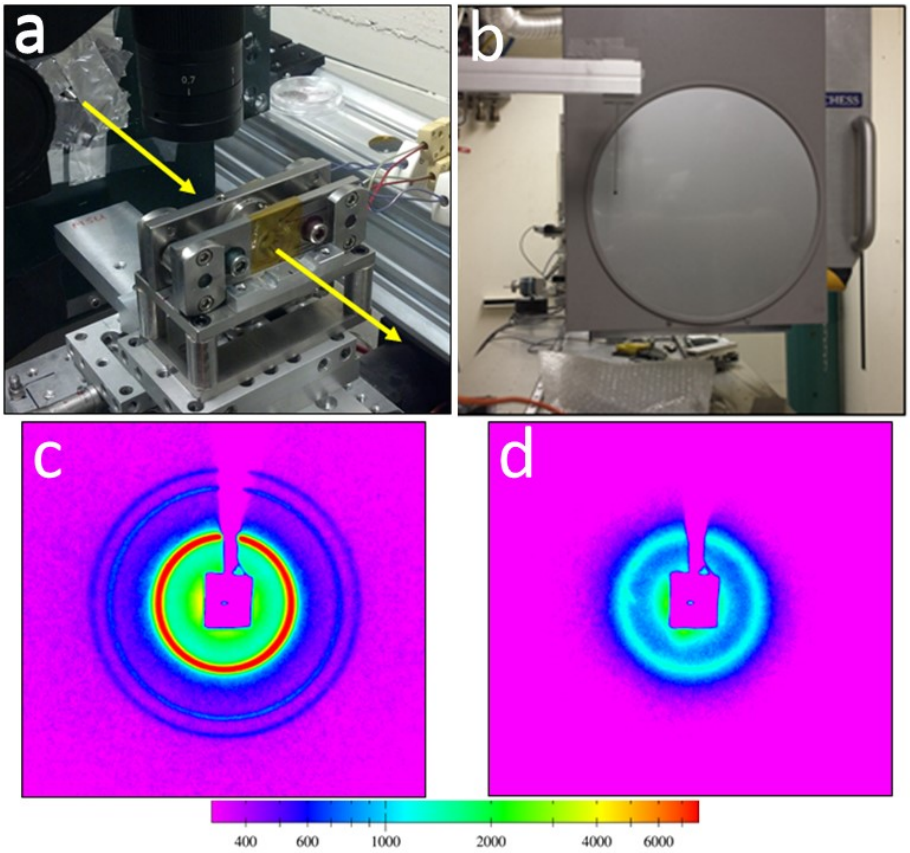

Figure 2.1: a) Experimental setup showing the DAC and mount used to support the DAC during SAXS measurements at beam line B1 of CHESS. The x-ray beam path through the sample in the DAC is indicated by the yellow arrows; b) MAR345 image plate detector used to measure the SAXS from the samples; 2D XRD images of Al-SBA15 at P = 0.1 GPa (c) and P = 2.1 GPa (d).

Computational Modeling

Classical molecular dynamics simulations were made on a box of 27,000 atoms representing the periodic SBA-15 type mesoporous silica and aluminosilica. Pores were cut out of each box of atoms in 2d-hexagonal pore symmetry conforming to the *p6mm* structure. The MD simulations were made at three pressures for mesoporous silica and aluminosilica ranging between 0.1 to 4.6 GPa. The size of the pores were varied in order to control the percent porosity. I used LAMMPS[18] software to run the MD simulations whereas Buckingham potentials were used for the Si-O, Al-O and O-O interactions.

Following the work of Du,[19] the Ewald Sum method was used to calculate the Coulombic interactions among the ionic constituents. The simulation cell was first elevated to 4000 K for 20 picoseconds, with a time step of 1 picosecond, to generate a melt. The melted cell was subsequently quenched from 4000 K to 300 K at a rate of 50 K/picosecond. Analysis of the radial distribution function (RDF) confirmed that the quenched simulation cell consisted of an amorphous structure. To discover the computer glass transition temperature (Tg) of the aluminosilica, the cell volume was plotted against temperature data for the quenching simulation from 4000 K to 300 K, and then the discontinuity in the trend of the slope was located.[20] The MD under simulated pressure were run at two temperature conditions: 300 K or at the calculated glass transition temperature (T_g). The T_g values were found to be 1800 K and 2400 K, as determined by the discontinuity point in the slope of the graph of cell volume vs temperature, for aluminosilica and silica, respectively. The simulations were made at T_g in order to accelerate the molecular dynamics and thus test whether formation of "frozen" states may have occurred under lower simulated temperature conditions, thus adversely affecting the compressibility of the cell under pressure. Hydrostatic pressure was exerted on the simulation cell of varying porosities to the point of reaching equilibrium in cell volume. The bulk modulus was calculated from the inverse of the linear slope determined from dependence of V_P/V_0 vs pressure, where V_P is the volume of the simulation cell at pressure and V_0 is the volume at 0.1 Mpa. By repeating this procedure for simulation boxes having varying pore volumes, the effect of porosity on the bulk modulus was determined using MD simulations. In order to expedite the simulations, supercomputing

and data storage facilties were used at the Extreme Science and Engineering Discovery Environment (XSEDE) and the Texas Advanced Computing Center (TACC).

Results and Discussion

In order to ascertain the morphological features and elemental composition of the mesoporous SBA-15 silica and the mesoporous Al-SBA-15 aluminosilica samples, SEM imaging and energy dispersive x-ray (EDX) spectroscopy were used. Presence of pores in the samples was verified from the SEM imaging. The SEM images show both samples exhibit a flake-like particulate appearance. The EDX measurements confirmed that the SBA-15 sample contained Si and O only whereas Al was detected in addition to Si and O for Al-SBA-15. Figure 2.2 shows TEM images of the mesoporous SBA-15 silica and the mesoporous Al-SBA-15 aluminosilica samples. As indicated from the TEM images, both materials poses highly ordered two-dimensional hexagonal symmetry pore structure; this is most evident where the cross sections of the pores are shown. Statistical analysis from the TEM images indicates that the mesoporous SBA-15 silica and the mesoporous Al-SBA-15 aluminosilica have pore diameters of 10.57±0.47 and 8.25±0.35 nm and pore wall thicknesses of 4.39±0.24 and 3.09±0.19 nm (within 1 σ), respectively. This leads to a percentage porosity of 45% for SBA-15 silica and 48% for Al-SBA-15 aluminosilica.

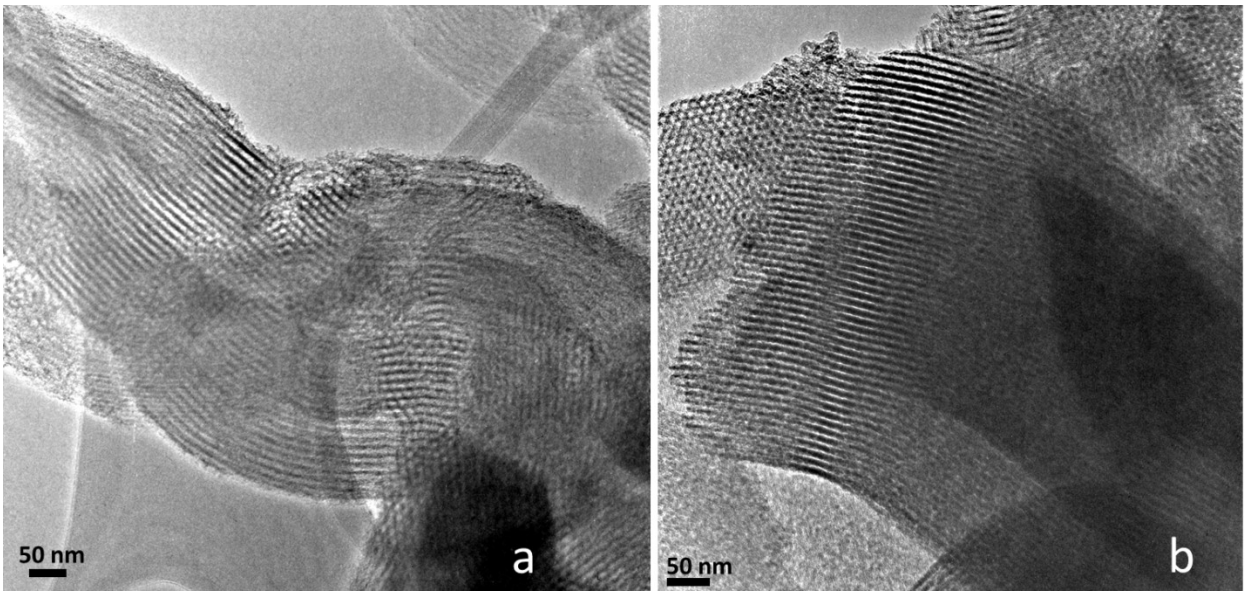

Figure 2.2: TEM images of mesoporous SBA-15 silica (a) and Al-SBA-15 aluminosilica samples (a). The scale bars are shown at the bottom of the images.

The XPS survey scans (shown in the Supplementary Information section) show that the chemical composition of SBA-15 silica is made up solely of Si and O and that the Al-SBA-15 aluminosilica chemical composition constitutes only Si, Al, and O. Figure 2.3 shows the high resolution XPS spectra of the Si 2p and O 1s peaks measured from the mesoporous SBA-15 silica and of the Si 2p, O 1s, and Al 2p peaks measured from the Al-SBA-15 aluminosilica. Fitting of the high resolution XPS data shown in Figure 2.3 indicates that charging was present during the measurement. The O1s peak is located at 532.8 eV and at 533.5 eV due to the Si-O bonding in SBA-15 silica and Al-SBA-15 aluminosilica, respectively. The 103.2 and 105.2 eV Si 2p peaks in SBA-15 silica and Al-SBA-15 aluminosilica, respectively, indicate that Si is in the 4+ oxidation state in both materials. Similarly, the 75.2 eV Al 2p XPS peak indicates that Al is in the 3+ oxidation state in Al-SBA-15 aluminosilica. Elemental analysis of the Si 2p, O 1s, and Al 2p peaks shows that there is 4.80 at% Al, 28.40 at% Si, and 66.80 at% O in the Al-SBA-15

aluminosilica; similar analysis of the Si 2p and O 1s peaks shows that there is 33.91 at% Si and 66.09 at% O in the SBA-15 silica.

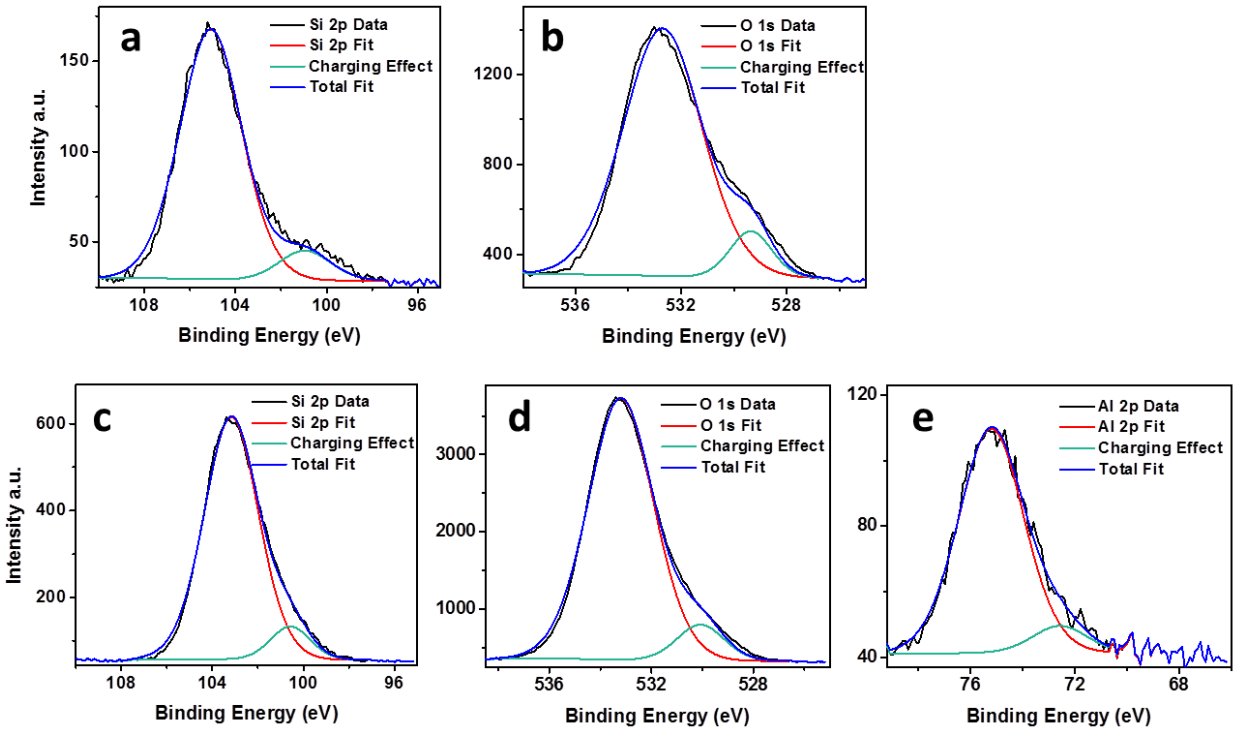

Figure 2.3: High resolution Si 2p (a) and O 1s (b) XPS data measured from the SBA-15 silica sample and high resolution Si 2p (c), O 1s (d), and Al 2p (e) XPS data measured from the Al-SBA-15 aluminosilica sample.

The *in situ* SAXS data measured as a function of pressure from the SBA-15 silica and the Al-SBA-15 aluminosilica are shown in Figure 2.4. The wide angle x-ray scattering (WAXS) data that were collected simultaneously with the SAXS only showed amorphous like atomic structure for both materials. The lattice parameter *a* of the 2-d hexagonal pore structure as determined from the room-temperature SAXS data is 15.3±0.1 nm and 11.6±0.1 nm for SBA-15 silica and the Al-SBA-15 aluminosilica, respectively. The mesoporous SBA-15 silica and the Al-SBA-15 aluminosilica have the

2d-hexagonal pore structure having *p6mm* space group symmetry as indicated by the presence of the (100), (110) and (200) reflection peaks. Deformation of the pore structure of both materials is evident by the diminution of the intensity of the SAXS peaks with increasing pressure. The progressive degradation in the ordering of the pore structure is most likely accompanied with a continuous reduction in pore size with increased pressure. The pore-structure deformation is more pronounced with pressure in SBA-15 silica than in Al-SBA-15 aluminosilica as evidenced by the complete disappearance of the SAXS for the former at 3.9 GPa whereas there is a small but discernable (100) peak of the SAXS present at 11.2 GPa for the latter material. The d_{100} spacing of the meso-scale structure, determined from fitting of the background subtracted SAXS (100) peak using a Gaussian peak shape, was used to calculate the pore lattice parameter (a) and the volume of the pore unit cell of the SBA-15 silica and the Al-SBA-15 aluminosilica.

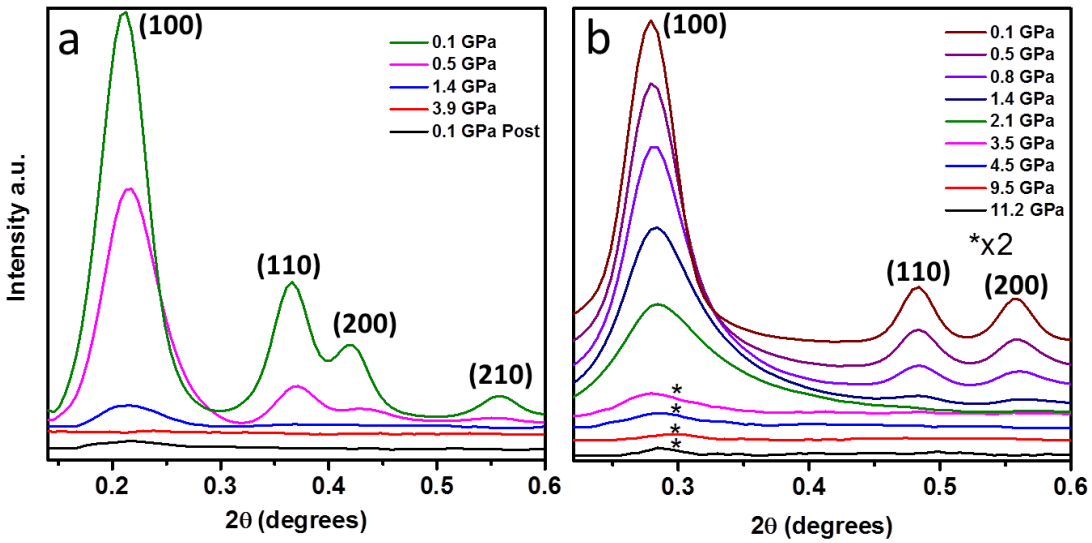

Figure 2.4: SAXS data as a function of 2θ measured from mesoporous SBA-15 silica (a) and Al-SBA-15 aluminosilica (b) as function of pressure.

The fractional value of the pore lattice volume at pressure normalized with respect to the volume under ambient pressure (V_P/V_0) was calculated in order to determine the bulk modulus of the SBA-15 silica and Al-SBA-15 aluminosilica. Figure 2.4 shows the variation of V_P/V_0 as a function of pressure for mesoporous SBA-15 silica and Al-SBA-15 aluminosilica. The bulk modulus, which is defined as $\kappa = -V\frac{dP}{dV}$, was determined from the inverse of the slope of the line fitted to the pressure-dependent V_P/V_0 data in the elastic region. For calculation of V, I used the approximation that the *c* parameter of a representative 3d-hexagonal like pore structure is equivalent to the *a* parameter of the 2d-hexagonal pore structure.

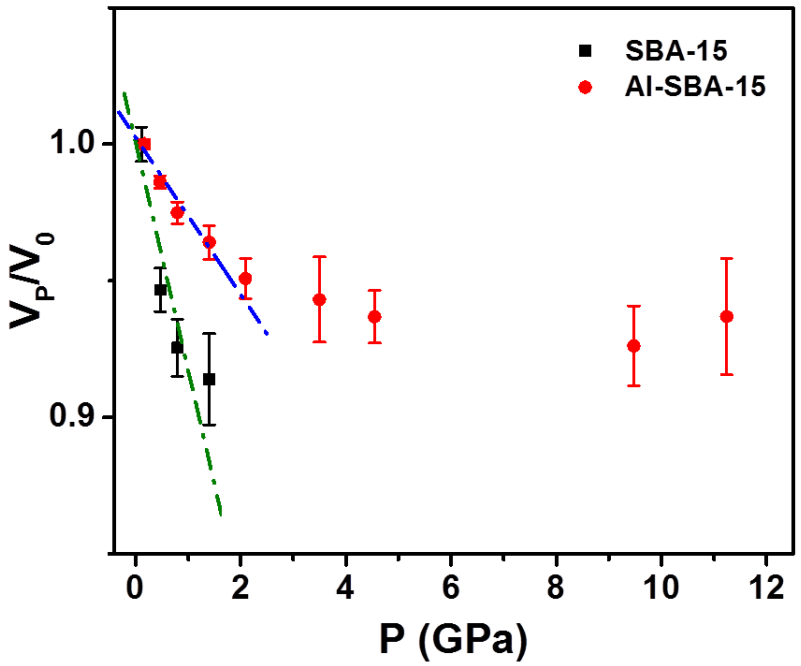

Figure 2.5: Fractional changes in volume of the mesopores (VP/V0) as a function of pressure (P). Bulk modulus (κ) is estimated from the linear fit made in the elastic region of the data.

Surprisingly, the estimated bulk modulus was found to be significantly different for the two materials. The Al-SBA-15 aluminosilica type periodic mesoporous material has a bulk modulus of 34.7±4.5 GPa, which is nearly three times the bulk modulus of the SBA-15 silica (12.0±3.0 GPa) mesoporous material. In Al-SBA-15, a significant portion of the Si^{4+} ions are replaced by Al^{3+} within the framework of the mesoporous architecture creating a local charge-imbalance. This may play a role in local strengthening within the predominantly amorphous-like atomic-scale structure, thereby enhancing the mechanical stability of mesoporous Al-SBA-15 aluminosilica as compared to SBA-15 silica. More discussion on this topic is made below.

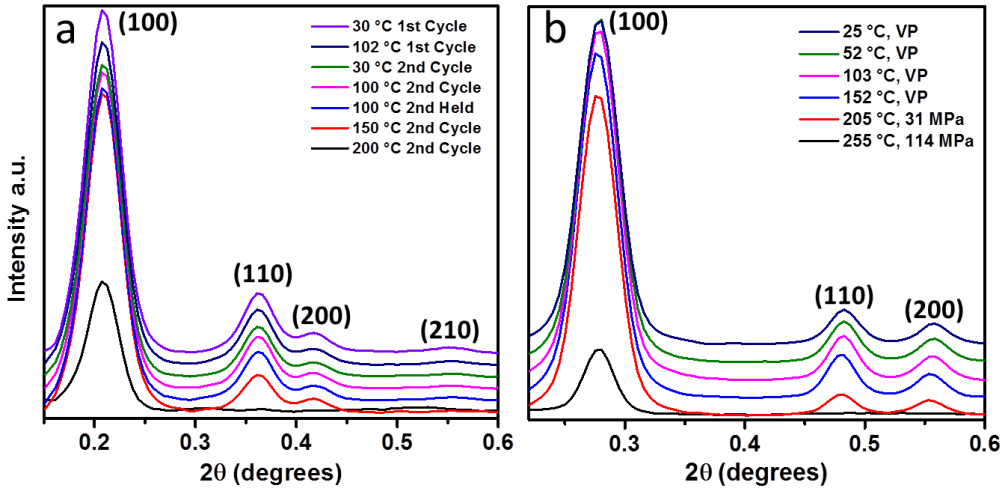

Figure 2.6: SAXS vs 2θ measured from mesoporous SBA-15 silica (a) and Al-SBA-15 aluminosilica (b) under extreme hydrothermal conditions. The operating pressures for the *in situ* SAXS of SBA-15 silica were all at vapor pressure (VP).

Figure 2.6 shows the in situ SAXS data measured under extreme hydrothermal conditions, to 200 °C and vapor pressure and 255 °C and 114 MPa, from the mesoporous SBA-15 silica and Al-SBA-15 aluminosilica samples, respectively. For the measurement run made on SBA-15 silica, two cycles were employed. The SAXS was first measured

from the sample at 30 and 102 °C after which the sample was cooled back to 30 °C and measured for the first cycle. For the second cycle, the sample was heated again and the SAXS was measured at sequentially greater temperatures except for extended measurements made at 100 °C (held for ~ 75 min).

In order to make an analysis of the *in situ* SAXS data measured from the samples under extreme hydrothermal conditions, it was necessary to determine the swelling of the mesoporous materials due to the dissolution of water within the pore walls. To assess the degree of swelling due to water incorporation into the frameworks, the contributions of volume change due to thermal expansion and volume contraction due to hydrostatic compression of the mesoporous materials were estimated and compensated for in my results. The coefficient of thermal expansion for fused silica[21] and for albite glass[22] were used to account for the change in the unit cell pore volume due to thermal expansion (V_T) using equation (1) shown below:

$$V_T = V_0(1+\alpha \cdot \Delta T) \tag{1}$$

Where V_0 is the unit cell pore volume under ambient conditions, α is the thermal expansion coefficient, and ΔT is the increase in temperature relative to room temperature (25 °C). The change (i.e., contraction) in the unit cell pore volume (V_P) due to increasing pressure was calculated using equation (2) shown below:

$$V_P = V_0(1-\frac{\Delta P}{\kappa}) \tag{2}$$

Here, κ is the bulk modulus of either the Al-SBA-15 aluminosilica or the SBA-15 silica and and ΔP is the increase in pressure relative to atmospheric conditions (~0.101 MPa).

Figure 2.7 shows the pore lattice volume expansion as a function of temperature, which reflects the swelling due to water dissolution into the pore walls of the SBA-15 silica and Al-SBA-15 aluminosilica, at higher P-T conditions. As observed from Figure 2.7, the rate of water incorporation into the framework is pronouncedly greater for the Al-SBA-15 aluminosilica than for the SBA-15 silica with temperature increase to ~ 150 °C.

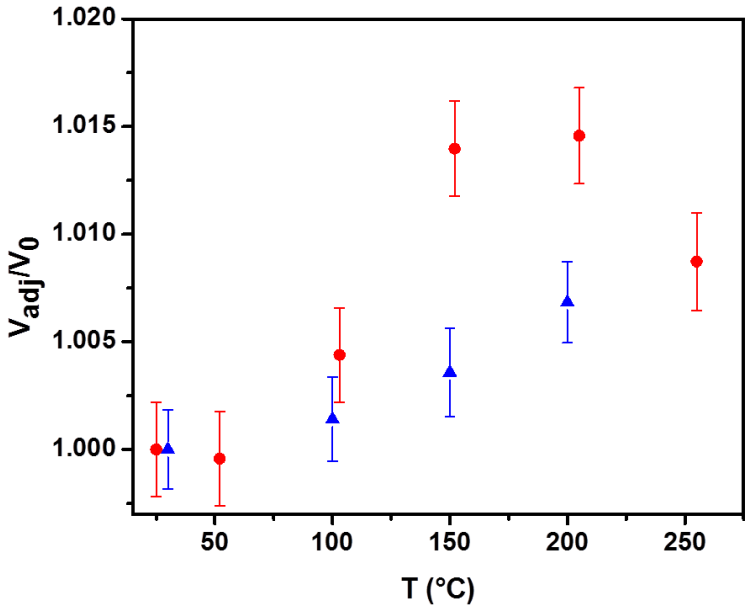

Figure 2.7: The pore lattice volume adjusted for thermal expansion and contraction due to pressure (Vadj) normalized to the value at ambient conditions (V0) as a function of temperature for SBA-15 silica (blue triangles) and for Al-SBA-15 aluminosilica (red circles).

However, as the temperature was increased beyond 150 °C, the pressure increased more significantly for Al-SBA-15 aluminosilica (up to 114 MPa) causing some degree of dehydration and reduction in swelling of the pore walls, leading to a partial recovery of the pore lattice volume from 200 to 255 °C. My results show an expansion of ~ 0.7% and ~ 1.5% of the pore lattice volume (i.e., swelling) at ~ 200 °C of the SBA-15 silica and of the Al-SBA-15, respectively, due to the dissolution of water into the framework of the

mesoporous materials under elevated P-T conditions. The reversal of the swelling beyond 205 °C and 31 MPa under hydrothermal conditions suggests that the dissolution of water in the pore walls is predominantly of the void filling type in mesoporous Al-SBA-15 aluminosilica.

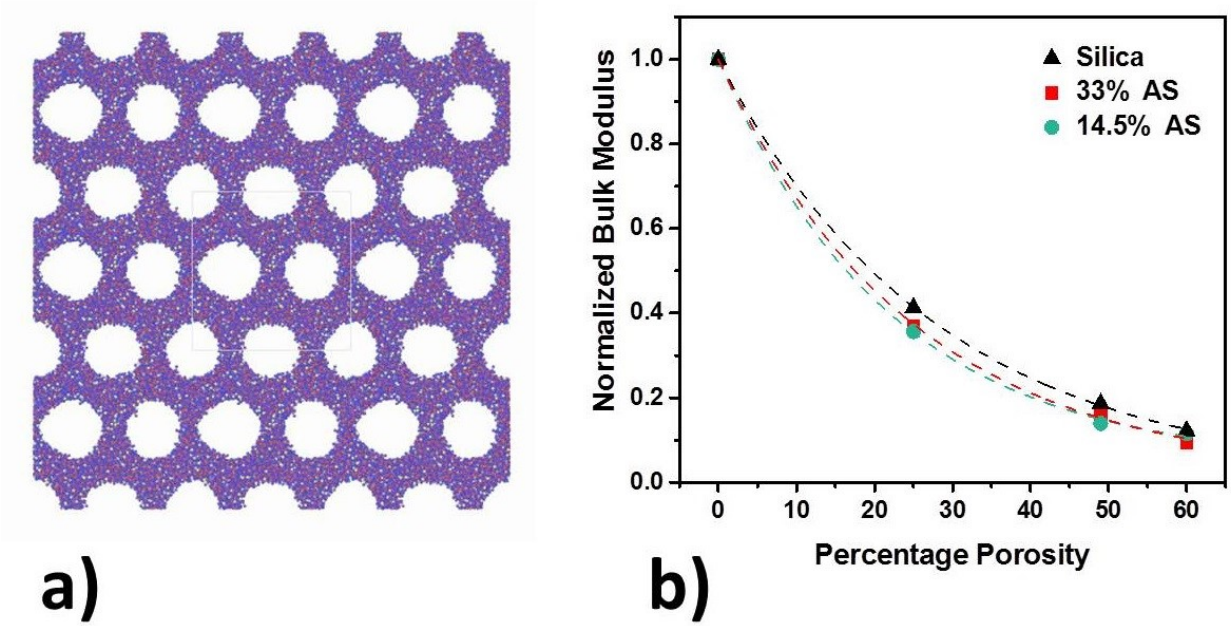

Figure 2.8: a) The simulation cell of the mesoporous Al-SBA-15 aluminosilica (with 33% Al content) having the 2D hexagonal pore structure with 49% porosity shown prior to MD simulation run, and b) bulk modulus values calculated from the MD simulations vs % porosity of the simulated SBA-15 silica (black symbol) and the Al-SBA-15 aluminosilica, having 14.5% (green symbol) and 33% Al content (red symbol). The dashed lines were obtained from fitting of the bulk modulus values with an exponential decay function of % porosity.

Molecular dynamics (MD) simulations were made of systems closely resembling the actual mesoporous SBA-15 silica and the Al-SBA-15 aluminosilica, in order to gain a better understanding of the mechanical properties and structure of the materials under pressure. The calculations were performed on simulation cells having various porosities, ranging from 0% (i.e., bulk) to 60%. For the simulation of mesoporous Al-SBA-15

aluminosilica, I constructed two different types of cells; one having a 14.5% and the other having a 33% Al (replacing Si) content, in order to test the effect of Al composition on the mechanical and structural properties. Figure 2.8 a) shows a simulation cell used for MD simulation of the mesoporous Al-SBA-15 aluminosilica (with 33% Al content) having the 2D hexagonal pore structure with 49% porosity. As shown in Figure 2.8b, the bulk modulus vs % porosity of the simulated SBA-15 silica and the Al-SBA-15 aluminosilica (for 14.5% and 33% Al content) have very similar exponential decay dependencies; this behavior is consistent with the mechanical stability of non-periodic and randomly porous materials. The usefulness of the plot shown in Figure 2.8b) is in the predictive capability of the reduction of bulk modulus with % porosity of the modeled material. If we use the experimentally determined bulk modulus value of 37.0 GPa for fused silica (i.e., quartz),[23] and the functional dependence shown in Figure 2.8b), I estimate that the bulk modulus of a 45% porosity SBA-15 type silica would be ~ 9 GPa. The predicted value of ~ 9 GPa is 25 % lower than my measured value for SBA-15 type silica (12.0 GPa). Although high albite ($NaAlSi_3O_8$) contains Na (typically with much lower K content), having a Al:Si ratio of 1:4, it is one of the better aluminosilicates that matches the Al:Si ratio of my Al-SBA-15 aluminosilica material. Using the experimental bulk modulus of 57.4 GPa of fused high albite as determined by Tenner et al.[24] and my K vs % porosity dependence shown in Figure 8 b), I estimate that the bulk modulus of a 48% porosity Al-SBA-15 type aluminosilica should be ~ 10 GPa. Thus, although the discrepancy between the predicted and experimentally measured bulk modulus values for SBA-15 type silica is reasonable, I see that the discrepancy (> 70%) for Al-SBA-15 aluminosilica is very large. Thus, my calculations appear not be completely accurate in

modeling of the mechanical properties of the Al-SBA-15 aluminosilica. My conjecture is that there may be additional atomic scale structural properties of the Al-SBA-15 aluminosilica framework that have yet to uncovered. A recent nuclear magnetic resonance (NMR) study by Ren et al.[25] showed evidence for intermediate range atomic-scale order in Al_2O_3-SiO_2 glasses prepared using sol gel techniques, which, in principle bear much similarity to the surfactant aided self-assembly procedures used to synthesize Al-SBA-15 aluminosilica. The presence of intermediate range atomic order would have a significant bearing on the compressibility of aluminosilica material in the mesoporous arrangement. In addition, it is not known to what extent potential hydroxylation of the non-bridging oxygens in the aluminosilica framework may play a role in affecting the mechanical properties of Al-SBA-15 aluminosilica. Charge compensation through the addition of H, Na, K, etc. are suggested as future directions for research, both by computational and experimental means, of mesoporous aluminosilica materials. In addition, detailed magic angle spinning nuclear magnetic resonance (MAS-NMR) analysis is suggested in order to obtain data on the local structure and potentially intermediate structure of Al-SBA-15 aluminosilica.

Conclusions

The bulk modulus of periodic mesoporous Al-SBA-15 aluminosilica having a 2d hexagonal pore lattice structure has been determined to be 34.7 ± 6.5 GPa. This is more than twice the bulk modulus (12.0 ± 3.0 GPa) of a periodic mesoporous SBA-15 silica having the same 2d hexagonal pore lattice structure. I conjecture that the replacement of Si^{4+} by Al^{3+} within the atomic network that constitutes the framework may play a role in enhancing the mechanical stability of mesoporous Al-SBA-15 aluminosilica as compared

to that of mesoporous SBA-15 silica. I find that there is an expansion of the pore lattice volume of mesoporous SBA-15 silica by 0.7 % and of mesoporous Al-SBA-15 aluminosilica by 1.5 % at ~ 200 °C due to the dissolution of water into the framework of these mesoporous materials under elevated P-T conditions. My molecular dynamics simulations show that the bulk modulus values of simulated mesoporous SBA-15 silica and Al-SBA-15 aluminosilica (both for 14.5 and 33 % Al vs Si content) vary exponentially with percentage porosity in much the same manner with respect to each other and as for non-periodic and randomly porous materials. The discrepancy between the experimental results and the computational modeling may be due to as yet unexplored structural characteristics, such as the presence of intermediate range atomic order or charge compensation by hydroxylation, of the mesoporous Al-SBA-15 aluminosilica.

Acknowledgments

DK acknowledges support from the NASA-MO space grant. We thank Rishi Patel for performing the XPS measurements at the JVIC center of Missouri State University.

References

1.A. G. Slater and A. I. Cooper: Function-led design of new porous materials. *Science* **348**(6238), aaa8075 (2015).

2.C. T. Kresge and W. J. Roth: The discovery of mesoporous molecular sieves from the twenty year perspective. *Chem. Soc. Rev.* **42**(9), 3663 (2013).

3.Y. Yamauchi, N. Suzuki, L. Radhakrishnan, and L. Wang: Breakthrough and future: nanoscale controls of compositions, morphologies, and mesochannel orientations toward advanced mesoporous materials. *Chem. Rec.* **9**(6), 321 (2009).

4.G. J. de AA. Soler-Illia, C. Sanchez, B. Lebeau, and J. Patarin: Chemical strategies to design textured materials: from microporous and mesoporous oxides to nanonetworks and hierarchical structures. *Chem. Rev.* **102**(11), 4093 (2002).

5.M. E. Davis: Ordered porous materials for emerging applications. *Nature* **417**(6891), 813 (2002).

6.R. A. Mayanovic, H. Yan, A. D. Brandt, Z. Wang, M. Mandal, K. Landskron, and W. A. Bassett: Mechanical and hydrothermal stability of mesoporous materials at extreme conditions. *Microporous Mesoporous Mater.* **195**, 161 (2014).

7.J. Wu, X. Liu, and S. H. Tolbert: High-pressure stability in ordered mesoporous silicas: Rigidity and elasticity through nanometer scale arches. *J. Phys. Chem. B* **104**(50), 11837 (2000).

8.R. Mokaya: Synthesis of Mesoporous Aluminosilicates with Enhanced Stability and Ion-Exchange Capacity via a Secondary Crystallization Route. *Adv. Mater.* **12**(22), 1681 (2000).

9.Y. Han, S. Wu, Y. Sun, D. Li, F.-S. Xiao, J. Liu, and X. Zhang: Hydrothermally Stable Ordered Hexagonal Mesoporous Aluminosilicates Assembled from a Triblock Copolymer and Preformed Aluminosilicate Precursors in Strongly Acidic Media. *Chem. Mater.* **14**(3), 1144 (2002).

10.K. Wang, Y. Lin, M. A. Morris, and J. D. Holmes: Preparation of MCM-48 materials with enhanced hydrothermal stability. *J. Mater. Chem.* **16**(41), 4051 (2006).

11.D. Zhao, Q. Huo, J. Feng, B. F. Chmelka, and G. D. Stucky: Nonionic Triblock and Star Diblock Copolymer and Oligomeric Surfactant Syntheses of Highly Ordered, Hydrothermally Stable, Mesoporous Silica Structures. *J. Am. Chem. Soc.* **120**(24), 6024 (1998).

12.S. Wu, Y. Han, Y.-C. Zou, J.-W. Song, L. Zhao, Y. Di, S.-Z. Liu, and F.-S. Xiao: Synthesis of Heteroatom Substituted SBA-15 by the "pH-Adjusting" Method. *Chem. Mater.* **16**(3), 486 (2004).

13.G. L. Athens, D. Kim, J. D. Epping, S. Cadars, Y. Ein-Eli, and B. F. Chmelka: Molecular Optimization of Multiply-Functionalized Mesoporous Films with Ion Conduction Properties. *J. Am. Chem. Soc.* **133**(40), 16023 (2011).

14.A. P. Hammersley: FIT2D: an introduction and overview. *Eur. Synchrotron Radiat. Facil. Intern. Rep. ESRF97HA02T* (1997).

15.W. Wagner and A. Pruß: The IAPWS Formulation 1995 for the Thermodynamic Properties of Ordinary Water Substance for General and Scientific Use. *J. Phys. Chem. Ref. Data* **31**(2), 387 (2002).

16.C. A. Schneider, W. S. Rasband, and K. W. Eliceiri: NIH Image to ImageJ: 25 years of image analysis. *Nat. Methods* **9**(7), 671 (2012).

17.D. G. Kizzire, J. Thomas, S. Dey, H. Osman, R. A. Mayanovic, R. Sakidja, Z. Wang, M. Mandal, and K. Landskron: Investigations of the Mechanical and Hydrothermal Stabilities of SBA-15 and Al-SBA-15 Mesoporous Materials. *MRS Adv.* **FirstView**, 1 (2016).

18.S. Plimpton: Fast parallel algorithms for short-range molecular dynamics. *J. Comput. Phys.* **117**(1), 1 (1995).

19.J. Du: Molecular Dynamics Simulations of the Structure and Properties of Low Silica Yttrium Aluminosilicate Glasses. *J. Am. Ceram. Soc.* **92**(1), 87 (2009).

20.N. A. Morgan and F. J. Spera: Glass transition, structural relaxation, and theories of viscosity: A molecular dynamics study of amorphous CaAl2Si2O8. *Geochim. Cosmochim. Acta* **65**(21), 4019 (2001).

21.W. Souder: Measurements on the Thermal Expansion of Fused Silica (National Bureau of Standards, 1925).

22.J. Arndt and F. Häberle: Thermal expansion and glass transition temperatures of synthetic glasses of plagioclase-like compositions. *Contrib. Mineral. Petrol.* **39**(2), 175 (1973).

23.C. Meade and R. Jeanloz: Frequency-dependent equation of state of fused silica to 10 GPa. *Phys. Rev. B* **35**(1), 236 (1987).

24.T. J. Tenner, R. A. Lange, and R. T. Downs: The albite fusion curve re-examined: New experiments and the high-pressure density and compressibility of high albite and NaAlSi3O8 liquid. *Am. Mineral.* **92**(10), 1573 (2007).

25.J. Ren, L. Zhang, and H. Eckert: Medium-Range Order in Sol–Gel Prepared Al2O3–SiO2 Glasses: New Results from Solid-State NMR. *J. Phys. Chem. C* **118**(9), 4906 (2014).

Supporting Information

Studies of the Mechanical and Extreme Hydrothermal Properties of Periodic Mesoporous Silica and Aluminosilica Materials

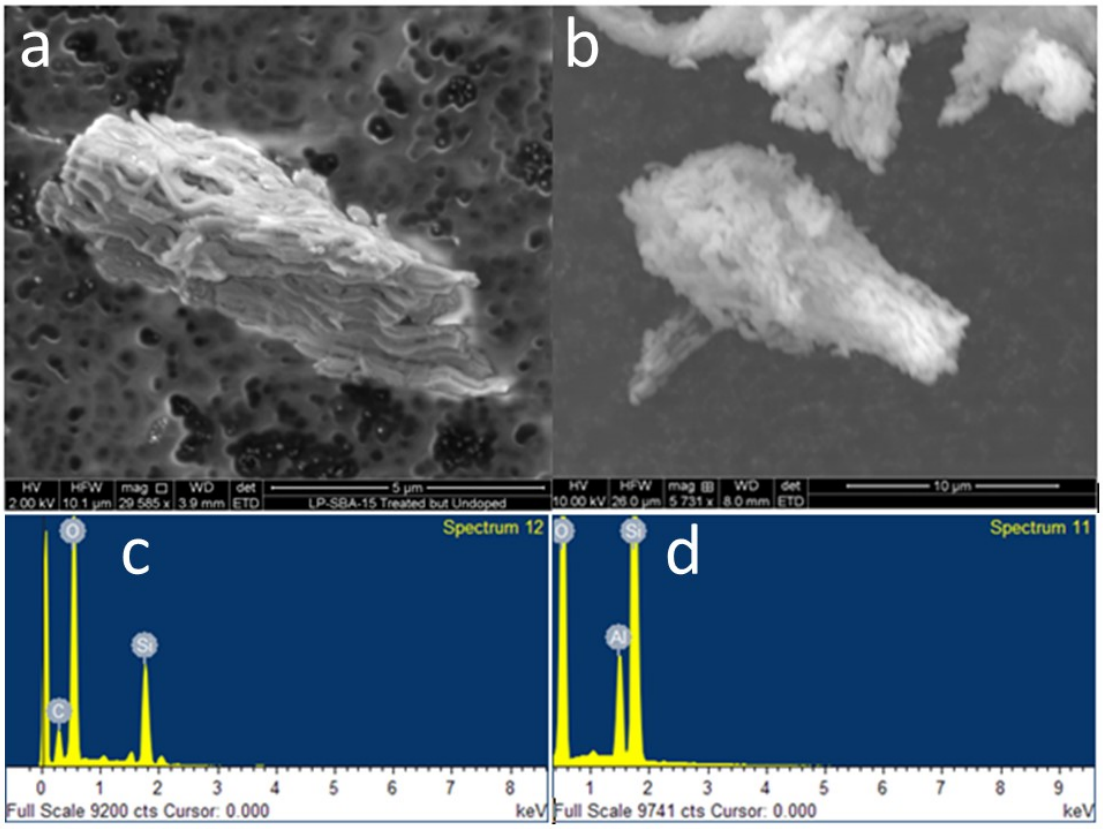

Figure S1: SEM images of mesoporous SBA-15 silica (a) and Al-SBA-15 aluminosilica samples (a). The scale bars are shown at the bottom of the figures. EDX measurements of SBA-15 silica (c) and Al-SBA-15 aluminosilica (d).

DYNAMICS STUDY OF THE MECHANICAL PROPERTIES OF SIMULATED PERIODIC MESOPOROUS SILICA AND ALUMINOSILICA

Abstract

Porous silica and aluminosilica glasses are important technological materials for heterogeneous catalysis, biomass gasification, gas sensing, and filtering due to their tunable pore sizes and high surface area to volume ratio. It is necessary for these materials to possess a great structural stability in order to survive the extremely harsh conditions for industrial applications. I have made classical molecular dynamics simulations of silica and charge uncompensated aluminosilica amorphous glasses with varying percentage porosity with a simulated 2D hexagonal pore structure, chemical composition, and onset of pressure at varying temperatures. This work also includes an in-depth analysis of the dependence of the bulk modulus with percent porosity and bond angle deformations under hydrostatic pressure. Two types of pressure analysis techniques were explored, 1) pressure onset at computer-glass transition temperature, and, 2) pressure onset at room temperature. For these two types of pressure analyses, the percentage porosity was varied from 0% to 60% and the chemical composition was changed in the percentage of Al^{3+} substituted for Si^{4+} from 0% (bulk silica) to 33%. The results show a decrease of the bulk modulus with respect to increasing percentage porosity that follows an exponential decay curve, which is consistent with experimental data on randomly porous materials. The results also show a bimodal distribution of the bond angles for the charge uncompensated aluminosilica suggestive of edge sharing of

adjacent tetrahedra from the local charge imbalance created by substitution of the Al^{3+} ions.

Introduction

Silica-based amorphous or disordered materials are an important for wide ranging industrial and practical applications. Unlike for crystalline solids, the computational description of the mechanical properties, such as the compressibility and the Young's modulus, of amorphous materials poses more of a challenge. Very little is known about the structural deformation of mesoporous silica and aluminosilica and how the periodic pore structure affects the overall stability of the material. For ordered porous structures, it is important to note that there are two types of pores: open or interconnected cell pores and closed cell pores. The computational silica and aluminosilica that are studied here are periodically spaced porous structures on the mesoscale with closed cells that simulate the p6mm space group of SBA-15 silica and Al-SBA-15 aluminosilica: Both of these mesoscale structures have been previously studied.[1] The synthesis of mesoporous aluminosilicate (AS) materials using sol-gel techniques are typically conducted at slightly elevated temperatures in atmosphere; provided that a similar synthesis is made, but either under vacuum or inert atmosphere (e.g. argon,) the resultant mesoporous AS material should have similar structural properties to my calculations of a charge uncompensated material.

The molecular dynamic (MD) simulations of periodic mesoporous silica and aluminosilica are of vital importance for analyzing the structural strength, pore wall deformation, and net change of the surface area to volume ratio. These play a direct role in controlling the effective number of catalysis sites and thereby the catalytic activity of

the materials. Temperature studies are of such great significance for the mesoporous nanomaterials because temperature may strongly govern the mechanical properties of these amorphous mesoporous materials and many projected applications for these materials are likely to involve extreme pressure and temperature conditions required for maximum efficiency. There are a number of knowledge gaps in the understanding of the mechanical properties of ordered mesoporous materials: 1) the role of pore architecture, that is the type of periodicity and shape of the pores, 2) the effect of the percentage porosity of the structure, 3) the effect of the compositional atoms and ions of the material, and 4) the role of nanoscale defects including nano-grain boundaries and dislocations. All of these factors may play an important role for potential applications in the areas of heterogeneous catalysis, refractories, fuel cells, thermal insulations, gas sensing, high temperature filters, and biomass gasification.[1–4]

The goal of this study is to examine the mechanical properties of ordered mesoporous silica and aluminosilica having a 2d hexagonal pore structure, for varying composition in aluminosilica and for varying porosities. The calculation of the bulk modulus of silica and aluminosilica glasses is dependent upon many parameters that need to be optimized in order to achieve the most realistic results. These parameters include the distribution of Al atoms in the AS structure, glass formation, quench rate when cooling from a melt to form the glass, temperature of the system at the onset of pressure, and the relaxation of the systems.

Simulation Details

Forming the Amorphous Bulk Aluminosilica and Silica. Modeling the aluminosilica material, I first started with a crystalline SiO_2 (quartz) model cell

containing 27,000 atoms in which ⅓ of the silicon ions were replaced with aluminum ions at randomized positions. To preserve a charge neutral system, a stoichiometric calculation was completed and the resulting 1125 oxygen ions were removed leaving the aluminosilica system with a total of 25875 atoms. To effectively model the aluminosilica and silica materials, an Ewald[5] potential was used with Buckingham potential parameters.[5,6] The Buckingham pair coefficients between aluminum, silicon, and oxygen are shown in Table 1.

Table 1. Buckingham potentials used in the aluminosilica system.

Buckingham Potential Parameters			
Pairs	A (eV)	ρ (Å)	C (eV·Å)
$Si^{2.4}$ - $O^{-1.2}$	13,702.91	0.193817	54.681
$O^{-1.2}$ - $O^{-1.2}$	1,844.75	0.343645	192.58
$Al^{1.8}$ - $O^{-1.2}$	12,201.42	0.195628	31.997

It is well known that during the melt phase and quenching, the atom pairs can get too close to each other, causing problems in the Buckingham potential where the power term will override the exponential term effectively trapping atoms in a deep potential well.[5] Du et al. fixed this problem by splicing the Buckingham potential at short distances with a secondary function.[5,7,8] In the simulations, I applied the normal Buckingham potential without the use of such an additional function due to the relatively limited exposure of elevated temperatures that I used to generate the initial melt. In comparison, Du produced the melt at 6000 K for 160 ps whereas my melting process was made at only 4000 K for 20 ps, despite the fact that I utilized a higher number of statistics in the form of a larger number of atoms (my simulations having 27,000 atoms while Du et al.

used approximately 3000 atoms). Furthermore, I found no evidence of such trappings in the form of artificially short proximity of any atomic pairs. The individual pair distribution functions (PDFs) of each pair of atom types (Al-O, Al-Si, etc.) at room temperature exhibits a reasonable interatomic distance. The results were similar in the PDFs for the melts.

In order to determine the bulk modulus, structural properties, and the effects of periodic pore structure on amorphous silica and aluminosilica glasses, the crystalline aluminosilica simulation cell had to be melted and quenched to create a glass. To melt the aluminosilica, the cell was elevated to 4000 K for 20 picoseconds with a time step of 1 picosecond. The melted aluminosilica cell was quenched from 4000 K to 300 K at a rate of 50 K/picosecond totaling 74 picoseconds. Analysis of the radial distribution function (RDF) confirmed the end structure was indeed an amorphous glass.

To determine the computer glass transition temperature (Tg) of the aluminosilica, the cell volume was plotted against temperature data for the quenching simulation from 4000 K to 300 K, and then the discontinuity in the trend of the slope was located.[9] The discontinuity point in the slope is the temperature of Tg, which was found to be 1800 K and 2400 K for aluminosilica and silica respectively. Running the simulations at Tg accelerates the effective time of the simulation and prevents "frozen" states where the ions and tetrahedral units are locked into place and don't accurately respond to changes in pressure. [Citation]

Pressure Simulations. To effectively study the effect of temperature on the accuracy of the structural strength and bulk modulus of silica and aluminosilica, two types of simulations were made. The first (Type 1), with pressure being applied to the

bulk and porous materials while temperature was held at Tg, and the second type (Type 2) being that pressure on the simulation cells was applied after cooling from Tg and the system was at equilibrium at 300 K.

After the bulk glass was obtained at Tg, the next step was to carve the porous structure out of the bulk in order to study the effects of pore architecture and percentage porosity on structural strength. The pores were carved in the z-direction, going completely through the entire simulation cell, and arranged in an ABAB pattern in the x-y plane. This pore arrangement simulates the hexagonal periodic pore structure found in SBA-15 type silica and the Al-SBA-15 type aluminosilica. The simulation unit cell was configured to have four total pores by volume in a manner shown in Fig 3.1.

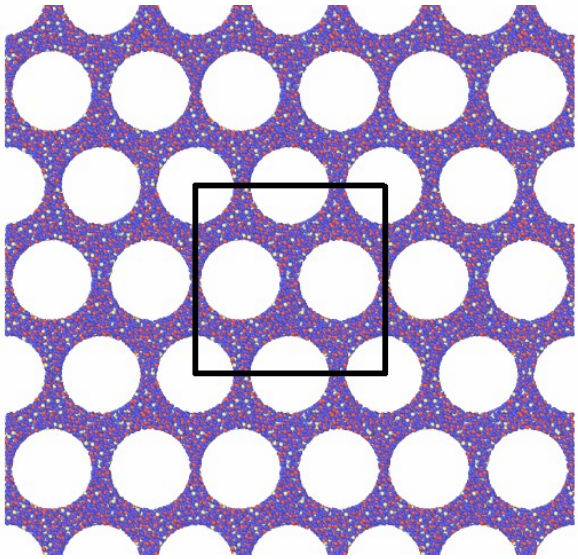

Figure 3.1: Schematic detailing the periodic pore structure and how the pores were carved from a cubic simulation cell.

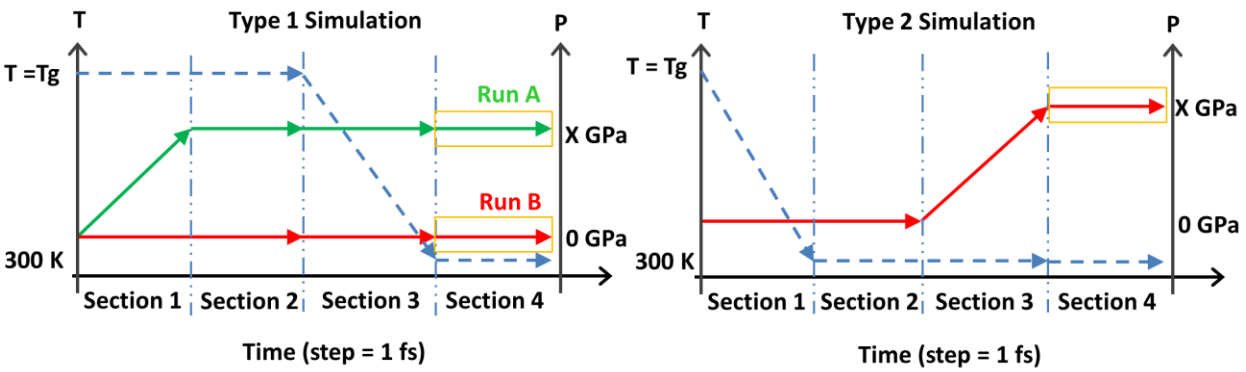

Figure 3.2: Type 1 and Type 2 simulation visualizations showing steps in the simulation process

Type 1 Simulation – Pressure Onset at Tg. The Type 1 simulations were split into four sections with two runs happening simultaneously. Both run A and run B were held at temperature Tg = 1800 K for aluminosilica, while run A had pressure linearly increased at a rate of 1 bar/fs to maximums of 1, 2, 2.5, and 4.5 GPa. In section 2, all of variables are kept constant allowing the simulation cell to reach equilibrium. Section 3 is the quenching stage where both Run A and Run B are quenched at a rate of 50 K/ps. Finally, Section 4 is the data collection stage where the pressure, temperature, and volume data of the simulation cells are averaged and plotted in order to determine structural stability, bulk modulus, bond angle distribution, and coordination number. Simulation Type 1 was applied to the silica material in the exact same manner with the only changes being constituent ions and Tg = 2400 K.

Type 2 Simulation – Pressure Onset at RT. The Type 2 simulations were also split into four sections. The Type 2 simulations were executed at Tg, then quenched to 300 K at a rate of 50 K/ps with 0 GPa of pressure on the cell. Section 2 is an equilibrium stage, followed by the pressure ramping stage, Section 3, in which the pressure is increased in the exact same way as Type 1 simulations to minimize any variables at play

in the simulations. Section 4 is again the data collection stage, where the pressure, temperature, and volume data of the simulation cell is averaged and plotted.

Varying Quench Rate. Both Type 1 and Type 2 simulations were ran a second time each for the bulk aluminosilica system, but instead of a 50 K/ps quench rate, the rate was halved to 25 K/ps in order to explore the effect of slower quenching times on the rigidity of the glass network and the structure of the pore walls. This did not produce any noticeably different results, so the 50K/ps quench rate was chosen for all of the simulations.

Results and Discussion

Fig. 3.3 shows a progression of frames of the aluminosilica simulation cell runs at pressures of 0 GPa (for Type 1 and Type 2), and at 1GPa and 2 GPa (Type 1) at 49% porosity in order to show the degradation of the framework structure and deformation of the pore wall architecture during equilibrium pressure stages of the simulation.

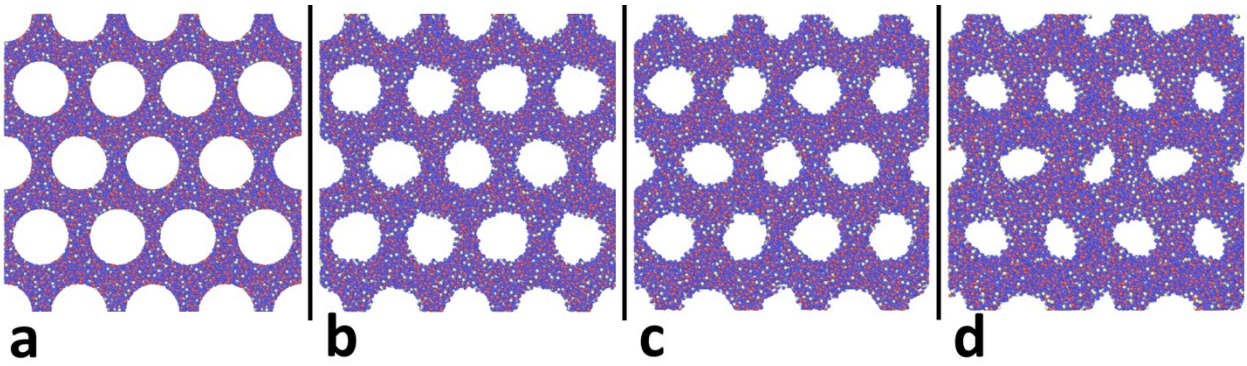

Figure 3.3: Progressive frames detailing pore wall deformation and volume change with increasing pressure. (a) 0 GPa at room temperature (RT) (b) 0 GPa at Tg (c) 1 GPa at RT (d) 2 GPa at RT.

In Fig. 3.3, frames (b), (c), and (d) are taken from the simulation at the end of the Type 1 run, when the simulation cells are at equilibrium pressure and have been

quenched to 300 K, except frame (a), which represents the aluminosilicate simulation cell directly after the pore structure is carved from the bulk. Frames (b), (c), (d) are at 0, 1, and 2 GPa respectively. The deformation of the pore walls can be seen clearly at 2 GPa as the sides of the pore walls start to flatten in places and the circular pores take on a more of an elliptical shape. Similar pore deformation is observed in the simulations of the 49% porosity silica with 2d hexagonal symmetry.

In order to numerically examine the effect that simulation temperature has on the pore architecture and the structural strength, bulk modulus calculations were performed for each simulation cell. To calculate the bulk modulus of the simulated material, the volume the simulation cell at pressure (Vp) was divided by the volume of the simulation cell with no pressure (V0). Each of the resultant normalized Vp/V0 values were plotted vs percent porosity and linearly fit. The inverse of the slope of the linear fit is the bulk modulus value. Figures 4 and 5 below show the Vp/V0 vs percentage porosity and bulk modulus variations of the silica and aluminosilica systems.

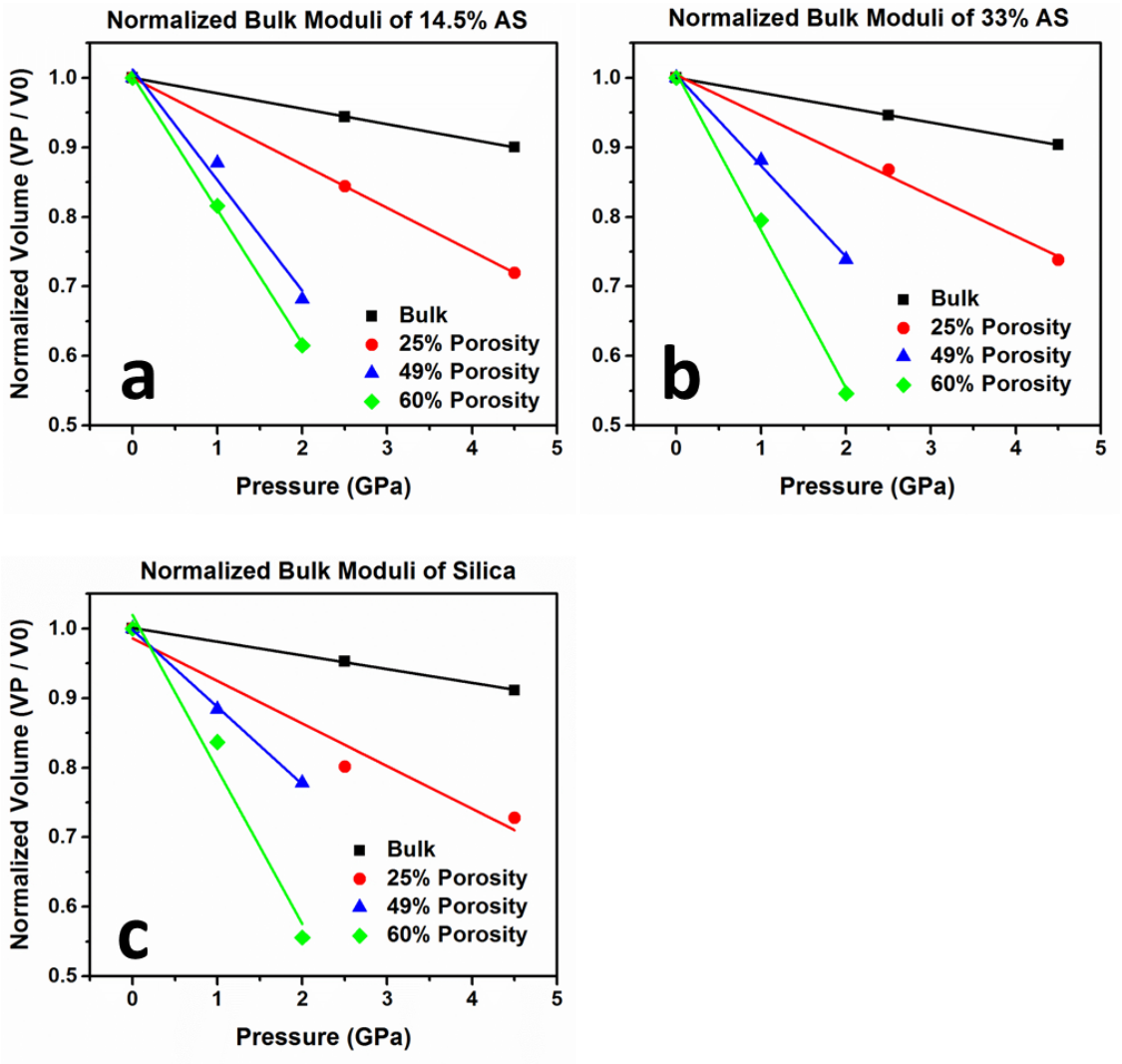

Figure 3.4: Normalized bulk moduli for Type 1 runs. (a) 14.5% AS (b) 33% AS (c) silica

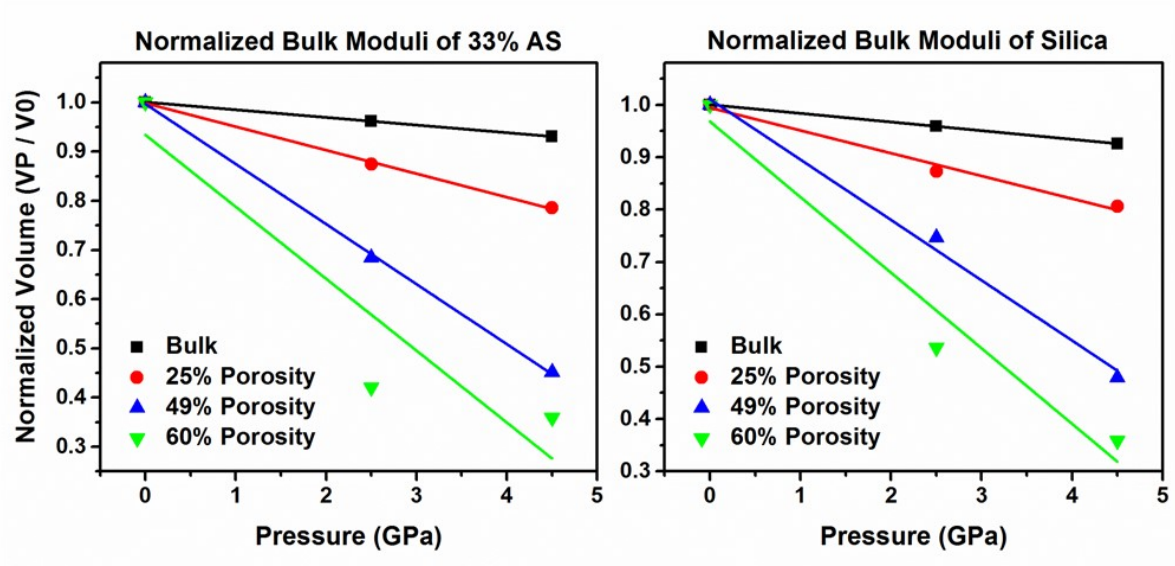

Figure 3.5: Normalized bulk moduli for Type 2 runs: (a) 33% AS and (b) silica.

Table 2 shows the bulk moduli values obtained for the four different percentage porosity simulation cells of silica and aluminosilica systems from the Type 1 and Type 2 runs.

Table 2 Bulk moduli values of the silica and aluminosilica systems of this study.

Bulk Moduli of Type 1 Runs (Gpa)			
% Porosity	14.5% Aluminosilica	33 % Aluminosilica	Silica
Bulk	45.02	46.66	53.76
25%	16.05	17.26	22.19
49%	6.28	7.65	10.02
60%	5.19	4.41	6.56

Bulk Moduli of Type 2 Runs (Gpa)		
% Porosity	33% Aluminosilica	Silica
Bulk	64.52	60.50
25%	20.94	23.05
49%	8.19	8.68
60%	6.84	6.92

These results seem to be consistent with respect to their measured mechanical properties of bulk fused silica[10] and bulk disordered albite type aluminosilica.[11] For Type 1 simulations, my calculated bulk moduli values seem to be 45% higher and 23% lower than the bulk moduli measured for fused silica and disordered albite, respectively. This is reasonable in lieu of the use of the Buckingham potentials to describe the interatomic

interactions in the materials.[5] I am in agreement with Du et al. who concluded that the potential well of the Si – O bond is stiffer as calculated using their potential parameters, when compared to experimental results.[5,12]

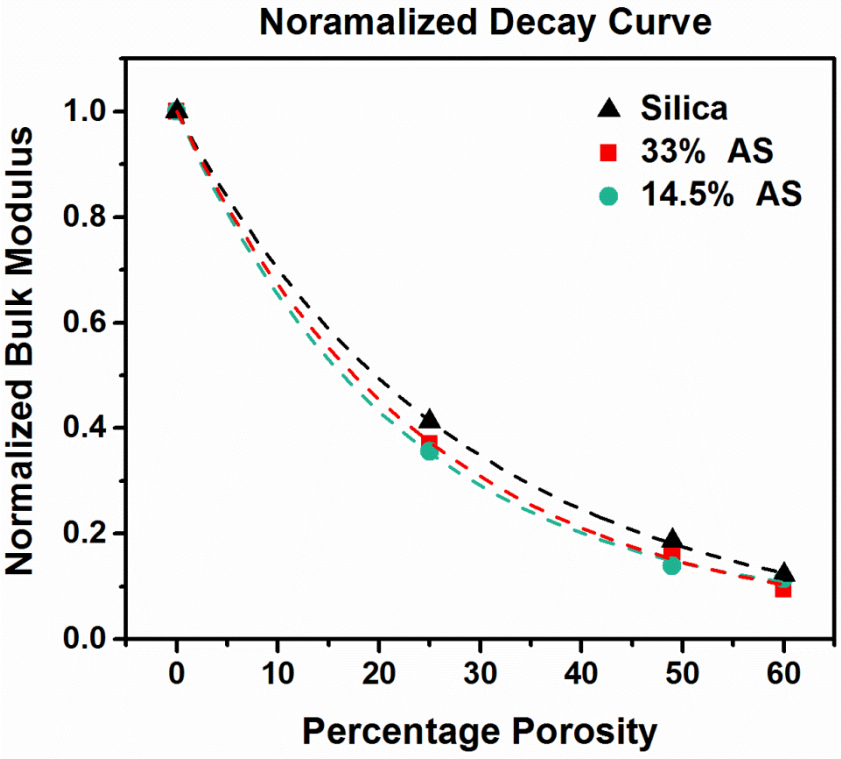

Figure 3.6: Normalized decay curve for silica (triangle), 33% aluminum cation AS (square), and 14.5% aluminum cation AS (circle).

Next, I compare the exponential dependence of the bulk modulus on the percent porosity for all three materials: silica, 14.5% aluminosilica, and 33% aluminosilica. In Figure 6 it can be clearly seen that there is an exponential dependence of normalized bulk modulus on the percentage porosity. The significance of the well-defined exponential dependence is that the structural strength of these materials can be very accurately estimated based on their percentage porosity.

The exponential decay observed in the normalized bulk modulus vs. percentage porosity plots in Figure 3.6 above is consistent with what is observed in randomly porous materials.[12] Also from Figure 3.6, it is evident that there is not much difference in the rate of decay between aluminosilica and silica, and furthermore there is negligible difference between the variation of the normalized bulk modulus with percentage porosity of the 14.5% AS vs the 33% AS. However, I note a discrepancy between my simulation results in that the predicted values based on the data shown in Figure 3.6 compare reasonably well for the measured bulk modulus of SBA-15 type silica but are in considerable disagreement with the measured bulk modulus of Al-SBA-15 type aluminosilica.[1] As was noted previously by our group (see Chapter 2), the discrepancy may be due to an intermediate range atomic scale ordering in the actual Al-SBA-15 type aluminosilica material or inaccurate atomic potentials for modeling of the mechanical properties of amorphous aluminosilica based systems.

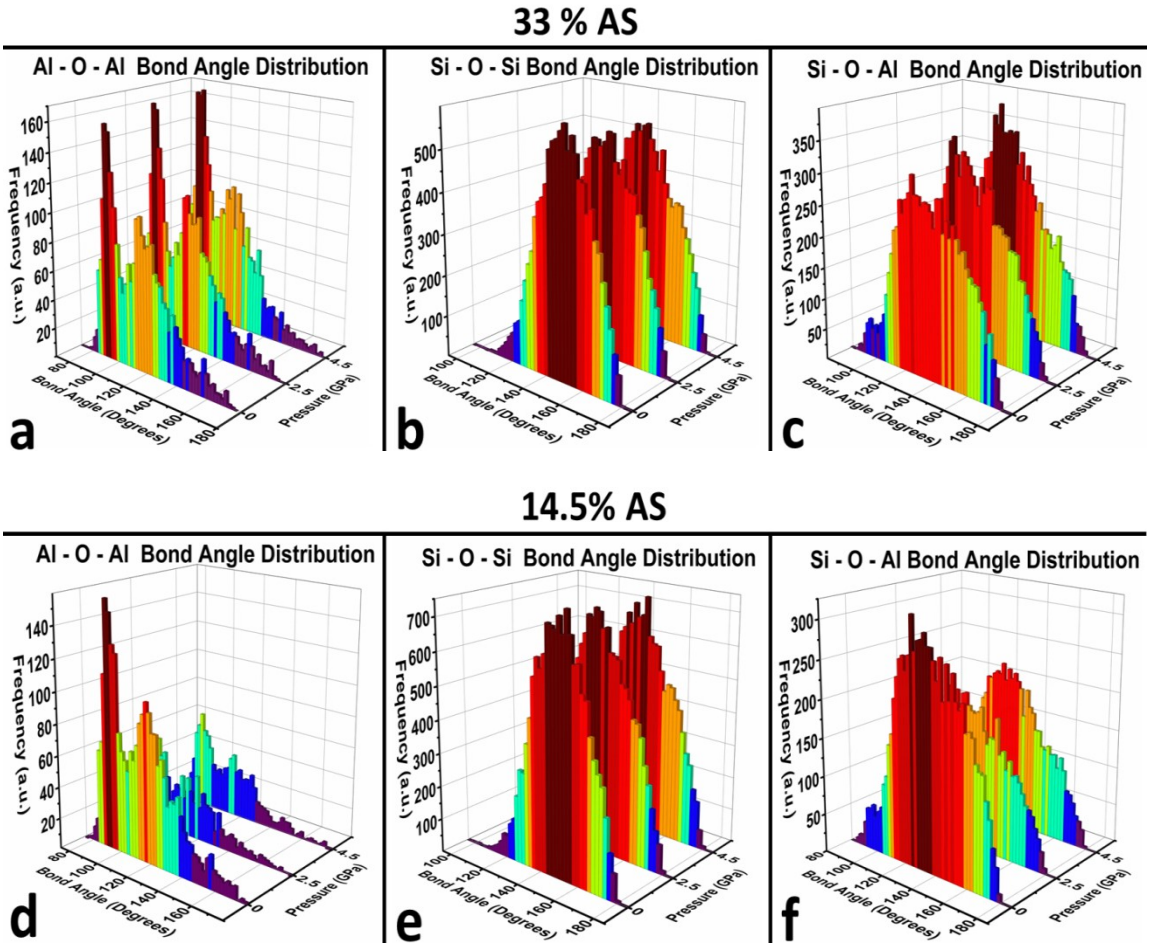

Figure 3.7: Al–O–Al (a), Al–O–Al (b), and Si–O–Al bond angle distributions for 33% Al content aluminosilica and Al–O–Al (a), Al–O–Al (b), and Si–O–Al bond angle distributions for 14.5% Al content aluminosilica simulations.

Figure 3.7 shows the bond angle (α) distributions of 33% AS between two adjacent tetrahedra connected via a bridging oxygen. Figure [3.7a, 3.7d] shows a bimodal distribution of the bond angles between tetrahedron with aluminum cations with peaks centered at 94° and 115°. I believe that this bimodal distribution is due to groupings of aluminum cations that form a local charge imbalance leading to edge sharing amongst the adjacent tetrahedra. This should only hold for a charge uncompensated AS material prepared in vacuum or inert atmosphere. The Si-O-Si bond angle is centered at 150° a

commonly accepted value[14] with increasing pressure rounding out the distribution as is expected.

Conclusions

The mechanical properties of the silica and aluminosilica are strongly driven by percentage porosity. As a corollary, for SBA-15 and Al-SBA-15, the decay of the normalized bulk modulus is exponential in roughly the same order which is quite similar to that of randomly porous materials; that is, the decay constant of the exponential dependence is roughly the same. The bimodal distribution of bond angles between tetrahedra of the aluminosilica may be due to edge sharing in the framework material created by local charge imbalances due to substitution of the Al^{3+} ions. This result should hold experimentally for a charge uncompensated aluminosilica material created in vacuum or inert atmosphere. Whereas my simulation results agree reasonably well in modeling the measured bulk modulus of SBA-15 type silica, the predicted values are in considerable disagreement with the measured bulk modulus of Al-SBA-15 type aluminosilica. It is conjectured that this may in part be due to inaccurate atomic potentials for modeling of the mechanical properties of the aluminosilica systems.

References

1. Kizzire, D. G. *et al.* Investigations of the Mechanical and Hydrothermal Stabilities of SBA-15 and Al-SBA-15 Mesoporous Materials. *MRS Adv.* 1–6 (2016). doi:10.1557/adv.2016.499

2. Alothman, Z. A. A review: Fundamental aspects of silicate mesoporous materials. *Materials (Basel).* **5,** 2874–2902 (2012).

3. Corma, A. From Microporous to Mesoporous Molecular Sieve Materials and Their Use in Catalysis. *Chem. Rev.* **97,** 2373–2419 (1997).

4. Magdeski, J. The porosity dependence of mechanical properties of sintered alumina. *J. Univ. Chem. Technol. Metall.* **45,** 143–148 (2010).

5. Du, J. Molecular dynamics simulations of the structure and properties of low silica yttrium aluminosilicate glasses. *J. Am. Ceram. Soc.* **92,** 87–95 (2009).

6. Du, J. & Cormack, A. N. Molecular dynamics simulation of the structure and hydroxylation of silica glass surfaces. *J. Am. Ceram. Soc.* **88,** 2532–2539 (2005).

7. Du, J. & Cormack, a. N. The structure of erbium doped sodium silicate glasses. *J. Non. Cryst. Solids* **351,** 2263–2276 (2005).

8. Du, J. & Corrales, L. R. Compositional dependence of the first sharp diffraction peaks in alkali silicate glasses: A molecular dynamics study. *J. Non. Cryst. Solids* **352,** 3255–3269 (2006).

9. Morgan, N. A. & Spera, F. J. Glass transition, structural relaxation, and theories of viscosity: A molecular dynamics study of amorphous CaAl2Si2O8. *Geochim. Cosmochim. Acta* **65,** 4019–4041 (2001).

10. Melorose, J., Perroy, R. & Careas, S. Frequency-dependent equation of state of fused silica to 10 GPa. *Statew. Agric. L. Use Baseline 2015* **1,** (2015).

11. T. J. Tenner, R. A. Lange, and R. T. Downs: The albite fusion curve re-examined: New experiments and the high-pressure density and compressibility of high albite and NaAlSi3O8 liquid. *Am. Mineral.* **92**(10), 1573 (2007).

12. Pedone, A., Malavasi, G., Cormack, A. N., Segre, U. & Menziani, M. C. Insight into elastic properties of binary alkali silicate glasses; Prediction and interpretation through atomistic simulation techniques. *Chem. Mater.* **19,** 3144–3154 (2007).

13. Rimsza, J. M. & Du, J. Structural and Mechanical Properties of Nanoporous Silica. *J. Am. Ceram. Soc.* **97,** 772–781 (2014).

14. Yuan, X. & Cormack, A. N. Si-O-Si bond angle and torsion angle distribution in vitreous silica and sodium silicate glasses. *J. Non. Cryst. Solids* **319,** 31–43 (2003).

CONCLUSIONS

This work has produced new knowledge and novel results that will benefit the design of mesoporous materials intended for energy applications in extreme environments. I have made *in situ* SAXS measurements of mesoporous SBA-15 silica and Al-SBA-15 aluminosilica, both having the two dimensional hexagonal pore structure with *p6mm* symmetry, under high pressures. The bulk modulus values determined from my SAXS measurements are 34.7 ± 4.5 GPa and 12.0 ± 3.0 GPa for mesoporous Al-SBA-15 aluminosilica and SBA-15 silica, respectively. This indicates that the Al-SBA-15 aluminosilica has much higher mechanical stability under hydrostatic pressure than the SBA-15 silica. My *in situ* SAXS study of the materials under extreme hydrothermal conditions (to 255 °C, 114 MPa) indicates that the Al-SBA-15 aluminosilica has greater hydrothermal stability than the SBA-15 silica. In addition, my characterization using *in situ* SAXS measurements has enabled a quantification of the amount of pore wall swelling of the SBA-15 silica and the Al-SBA-15 aluminosilica mesoporous frameworks undergo at specific temperature and pressure conditions of the supercritical aqueous environment. This provides a mechanism for the ultimate degradation in hydrothermal environments and is an important consideration for practical application of these mesoporous materials in near supercritical water/steam conditions.

The complementary computational classical molecular dynamics calculations have provided valuable insight into how the physiochemical properties, such as chemical composition and atomic scale structure, combine to govern the mechanical properties of periodic mesoporous silica and aluminosilica. Using readily available potentials and accounting for the variability of percentage porosity, chemical composition (in case of

SBA-15 type aluminosilica), and temperature at which pressure is applied, I have modeled the bulk modulus of many possible *p6mm* type silica and aluminosilica systems. My calculations show that the 2D SBA-15 type aluminosilica (irrespective of Al content) and the 2D SBA-15 type silica have very similar exponential-decay type functional relationship between bulk modulus and percent porosity, meaning that for nearly identical porosity values of the actual materials, their bulk modulus values should be much closer to each other than they are. This indicates that my calculations may not be completely accurate in modeling of the structural and chemical properties of the Al-SBA-15 type aluminosilica: Namely, there may be some level of intermediate range atomic-scale order or hydroxylation of the oxygen dangling bonds in the aluminosilica framework or the atomic potentials may not have the sufficient accuracy for modeling of the mechanical properties of these materials. The relationships between the bulk modulus and porosity and chemical composition (for mesoporous aluminosilica systems) developed from this work will allow researchers to estimate the structural strength of a mesoporous silica or aluminosilica based on the percentage porosity.

REFERENCES FOR OVERVIEW

1. R. A. Mayanovic, H. Yan, A. D. Brandt, Z. Wang, M. Mandal, K. Landskron, and W. A. Bassett: Mechanical and hydrothermal stability of mesoporous materials at extreme conditions. *Microporous Mesoporous Mater.* **195**, 161 (2014).

2. J. Wu, X. Liu, and S. H. Tolbert: High-pressure stability in ordered mesoporous silicas: Rigidity and elasticity through nanometer scale arches. *J. Phys. Chem. B* **104**(50), 11837 (2000).

3. P. Mohanty, V. Ortalan, N. D. Browning, I. Arslan, Y. Fei, and K. Landskron: Direct formation of mesoporous coesite single crystals from periodic mesoporous silica at extreme pressure. *Angew. Chem. Int. Ed.* **49**(25), 4301 (2010).

4. L. Zhang, P. Mohanty, N. Coombs, Y. Fei, H.-K. Mao, and K. Landskron: Catalyst-free synthesis of transparent, mesoporous diamond monoliths from periodic mesoporous carbon CMK-8. *Proc. Natl. Acad. Sci.* **107**(31), 13593 (2010).

5. X. H. Vu, R. Eckelt, U. Armbruster, and A. Martin: High-temperature synthesis of ordered mesoporous aluminosilicates from ZSM-5 nanoseeds with improved acidic properties. *Nanomaterials* **4**(3), 712 (2014).

6. C. T. Kresge, J. C. Vartuli, W. J. Roth, and M. E. Leonowicz: in *Stud. Surf. Sci. Catal.*, edited by O. Terasaki (Elsevier, 2004), pp. 53–72.

7. C. Liu, L. Li, H. Song, and X. Chen: Facile synthesis of ordered mesoporous carbons from F108/resorcinol–formaldehyde composites obtained in basic media. *Chem. Commun.* No. 7, 757 (2007).

8. K. P. Gierszal, T.-W. Kim, R. Ryoo, and M. Jaroniec: Adsorption and Structural Properties of Ordered Mesoporous Carbons Synthesized by Using Various Carbon Precursors and Ordered Siliceous P 6 mm and Ia $\bar{3}$d Mesostructures as Templates. *J. Phys. Chem. B* **109**(49), 23263 (2005).

9. P. Mohanty and K. Landskron: Synthesis of periodic mesoporous phosphorus–nitrogen frameworks by nanocasting from mesoporous silica using melt-infiltration. *J Mater Chem* **19**(16), 2400 (2009).